

# Paleo-Tethyan Oceanic Crust Subduction in the Eastern Section of the East Kunlun Orogenic Belt: Geochronology and Petrogenesis of the Qushi'ang Granodiorite

CHEN Guochao<sup>1,2</sup>, PEI Xianzhi<sup>1,\*</sup>, LI Ruibao<sup>1</sup>, LI Zuochen<sup>1</sup>, LIU Chengjun<sup>1</sup>,  
CHEN Youxin<sup>1</sup>, PEI Lei<sup>1,3</sup>, WANG Meng<sup>1</sup> and LI Xiaobing<sup>4</sup>

<sup>1</sup> Key Laboratory of Western China's Mineral Resources and Geological Engineering, Ministry of Education, Key Laboratory for the study of Focused Magmatism and Giant Ore Deposits, MLR, Faculty of Earth Science and Resources Chang'an University, Xi'an 710054, Shaanxi China

<sup>2</sup> Nanyang Institute of Technology, School of Civil Engineering, Nanyang 473000, Henan, China

<sup>3</sup> School of Earth Science and Resource, China University of Geosciences, Beijing 100083, China

<sup>4</sup> Shanxi Normal University, College of Geographical Sciences, Linfen 041000, Shanxi, China

**Abstract:** The Qushi'ang granodiorite (QSG) is located at the central east of the ophiolitic melange belt in the East Kunlun Orogenic Belt (EKOB) in the northern margin of the Qinghai-Tibetan Plateau. LA-MC-ICP-MS zircon U-Pb dating suggests that the granodiorite and mafic microgranular enclaves (MMEs) crystallized  $246.61 \pm 0.62$  and  $245.45 \pm 0.9$  Ma ago, respectively. Granodiorite, porphyritic diorite, and MMEs are metaluminous and medium-K calc - alkaline series, with island-arc magma features, such as LILE enrichment and HFSE depletion. The porphyritic diorite has high Cr (13.50 ppm to 59.01 ppm), Ni (228.53 ppm to 261.29 ppm), and Mg<sup>#</sup> (46–54). Granodiorite and porphyritic diorite have similar mineral compositions and evolved major and trace elements contents, particularly Cr and Ni, both of which are significantly higher than that in granites of the same period. The crystallization age of MMEs is close to that of granodiorite, and their major and trace elements contents are in-between porphyritic diorite and granodiorite. The results suggest that the original mafic magma, which was the product of mantle melting by subduction process, intruded into the lower crust (Kuhai Rock Group), resulting in the formation of granodiorite. Continuous intrusion of mafic magma into the unconsolidated granodiorite formed MMEs and porphyritic diorite. The granodiorite reformed by late-stage strike-slip faulting tectonic event indicates that the strike-slip fault of Middle Kunlun and the collision of the Bayanhar block with East Kunlun were later than 246 Ma. Therefore, the formation of the QSG not only indicates the critical period of evolution of East Kunlun but also represents the tectonic transition from oceanic crust subduction to slab breaking.

**Key words:** East Kunlun Orogenic Belt (EKOB), Qushi'ang granodiorite (QSG), mafic microgranular enclaves (MME), Early Triassic, Tibet, Proto-Tethy

## 1 Introduction

The Early Triassic was a significant period for the evolution of the East Kunlun Orogenic Belt (EKOB). The large-scale magmatism in the middle to late Early Triassic was responsible for the formation of large areas of granite (Liu Chengdong et al., 2004; Chen Hongwei et al., 2005; Li Bile et al., 2012; Zhang et al., 2012; Chen Guochao et

al., 2013a, 2013b, 2013c, 2016; Ding et al., 2014; Li et al., 2015; Ren et al., 2016). These granites are rich in mafic microgranular enclaves (MMEs) and intruded into a nearly E-W-trending East Kunlun fault. The granite in this area include diorite, granodiorite, granite, and syenogranite, which are considered the product of mantle-derived magmas at the base of the crust during subduction (Mo Xuanxue et al., 2007; Sun Yu et al., 2009; Xiong et al., 2014). However, Huang et al. (2014) argued that these

\* Corresponding author. E-mail: peixzh@sina.com

granites were products of partial melting of the oceanic crust during syncollision or postcollision extension (Ding et al., 2014).

The Qushi'ang granodiorite (QSG) is in the central East Kunlun ophiolitic melange belt in the eastern EKOB (Fig. 1). The QSG was initially thought to have crystallized during the Ordovician (Yin Hongfu et al., 2003). However, new data restrict the OSG within Early Triassic.

## 2 Regional Geology

The East Kunlun Orogenic Belt (EKOB) in the northern margin of the Qinghai-Tibetan Plateau is an important part of the Central Orogenic System (COS). It can be divided

into the northern East Kunlun tectonic belt, central East Kunlun ophiolitic melange belt, southern East Kunlun tectonic belt, and Buqingshan-A'nyemaqen ophiolitic belt from north to south (Yin Hongfu and Zhang Kexin, 1997; Xu Zhiqin et al., 2006, 2013; Meng et al., 2013; Pei Xianzhi et al., 2015; Zhang et al., 2016). The study area is located in the central East Kunlun ophiolitic melange belt in the eastern EKOB. The central East Kunlun fault is a large-scale tectonic belt cutting the lithosphere in the northern Qinghai-Tibetan Plateau and is also a large-scale deformation belt that separates the northern and southern East Kunlun belts along an east-west trend for approximately 1000 km. The central East Kunlun fault extends westward into Sinkiang near Tahebanri and

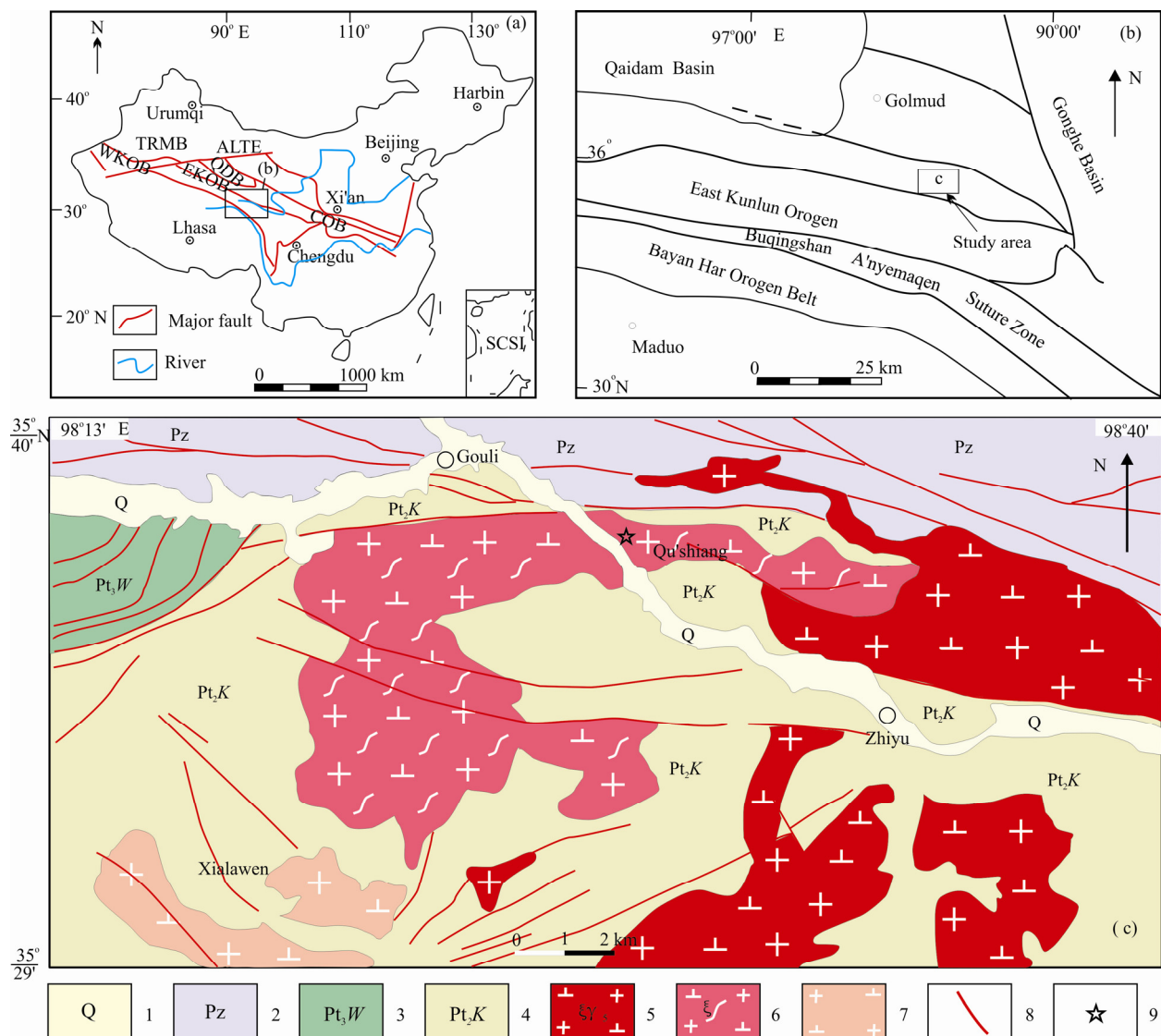


Fig. 1. (a) Map showing macroscopic tectonic framework of the Central Orogenic System (COS); (b) Tectonic units division of the EKOB and its adjacent area and (c) Geological sketch map of the Qushi'ang area in the eastern part of the EKOB.

ALTF, Altun sinistral strike-slip fault; EKOB, East Kunlun orogenic belt; QDB, Qaidam basin; TRMB, Tarim basin; WKOB, West Kunlun orogenic belt. 1. Quaternary; 2. Paleozoic; 3. Neoproterozoic Wanbaogou Group; 4. Kuhai Group of Changchengian; 5. Late Palaeozoic-Early Mesozoic granite; 6. Qushi'ang gneissic granodiorite; 7. Early Palaeozoic granite; 8. fault; 9. sampling locality

eastward to the northern hot springs and is cut by the Wahongshan dextral strike-slip fault. The Central East Kunlun fault underwent multiple geotectonic events resulting in complex and various structures, including pre-Cambrian metamorphic rock and plutons of variable age as well as ophiolite remnants.

The 30 km<sup>2</sup> QSG is in the south Qushi'ang in the central East Kunlun ophiolitic melange belt. The QSG was emplaced into the Meso-Proterozoic Kuhai Rock Group and was intruded by Late Triassic plutons in the east (Fig. 1). The QSG underwent ductile deformation based on its weakly gneissic. The QSG mainly comprises medium-to-fine grained granodiorite (Fig. 2a), which contains MMEs, and is intruded at its center by porphyritic diorite. The long axis of the MMEs varies between 10 and 30 cm, and while few are flat, most of them are oval in shape owing to intensive stretching (Fig. 2b).

### 3 Petrography

The granodiorite is grayish green to grayish, medium-to-fine grained, and weakly gneissic (Fig. 2a–c) and comprises plagioclase (40–45 vol%), K-feldspar (10–15 vol%), amphibole (10–15 vol%), quartz (15–20 vol%), and biotite (5 vol%). The plagioclase grains are euhedral columnar with dimensions of 0.5 mm × 1 mm to 1 mm × 2 mm and are zoned (Fig. 2c). The K-feldspar grains are subhedral with a perthitic texture. The amphibole grains

(0.8 mm–1.2 mm) are anhedral to subhedral with evident pleochroism and occasional twinning. Biotite is observed throughout the granodiorite, defining the weak foliation, and contains magnetite and apatite inclusions. The dark minerals form clusters (Fig. 2d) along shearing zones. Quartz commonly occurs as irregular grains in feldspar grains.

The dioritic MMEs are dark gray, fine-grained, weakly foliated and contain the same mineral assemblage as the host granodiorite (Fig. 2e).

### 4 Sampling and Analytical Methods

#### 4.1 Sampling

Fresh granodiorite, porphyritic diorite, and MME samples were collected in the southern Qushi'ang for analysis. Granodiorite (sample no. XRD050/8) and MME (sample no. XRD050/10) were collected for zircon U–Pb dating. The coordinates of these two samples are N35°38.201' and E98°26.586'. Fifteen samples, labeled and numbered XRD050/3, XRD050/5–6, XRD050/8–13, and XRD052/1–6, were collected for petrochemistry.

#### 4.2 Zircon U–Pb dating

The samples were crushed using conventional methods in the Regional Geological Mineral Research Institute of Langfang, Hebei Province. The zircons were sorted using conventional flotation methods. Subsequently, zircon

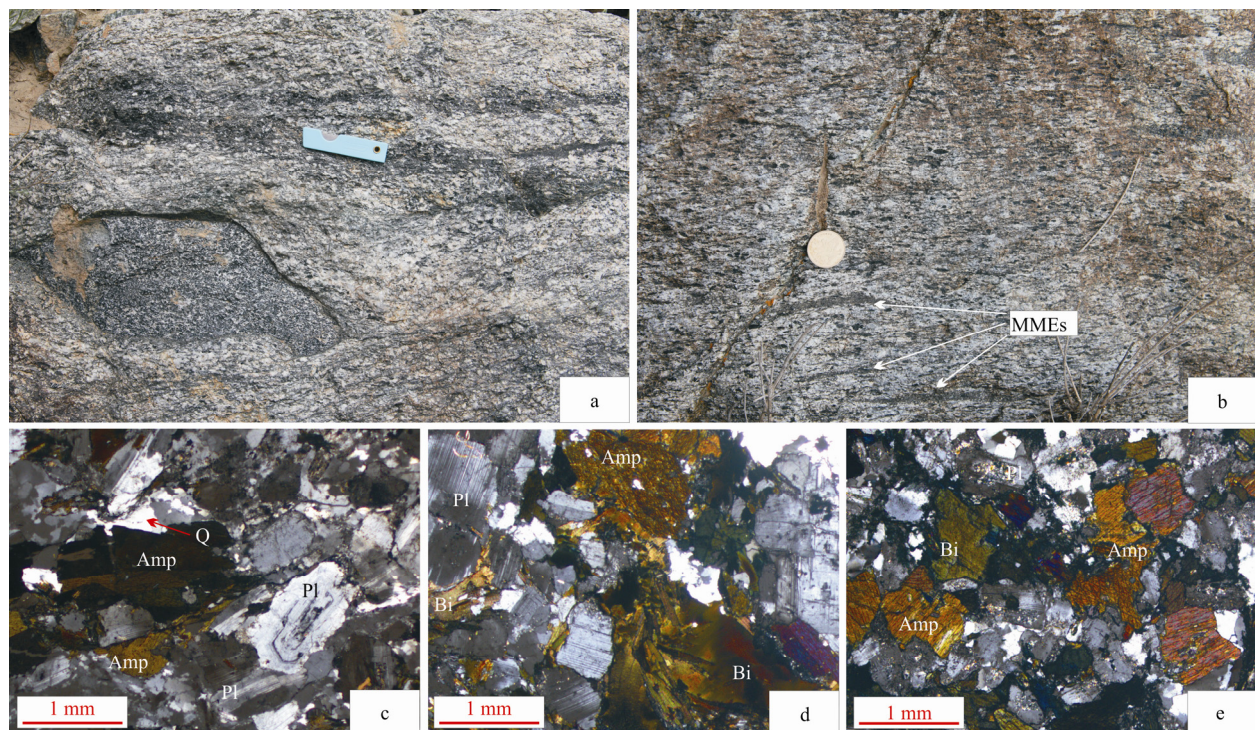


Fig. 2. Outcrop photos (a–b) and photomicrographs (c–e) of the typical textures from the QSG.  
Amp—amphibole, Pl—plagioclase, Bi—biotite, Q—quartz.

grains with good morphology and transparency were selected using a binocular microscope for analysis. The zircon grains were glued on double-sided tape, fixed with epoxy resin, and polished. Cathodoluminescence (CL) images were taken at the Beijing Zircon Navigation Technology Co., Ltd.

$U-Pb$  isotopic data were collected using a Neptune laser ablation multicollector plasma mass spectrometer (LA-MC-ICP-MS) at the Isotope Laboratory of Tian Jin Institute of Geology and Mineral Resources. The analytical methodology is that of Li Huaikun et al. (2010). The ISOPLOT 2.49 software was used in the age calculations and data plotting. The error in all data points is  $1\sigma$ . The weighted average of the  $^{206}\text{Pb}/^{238}\text{U}$  is given at a confidence level of 95% (Anderson, 2002; Ludwig, 2003).

#### 4.3 Geochemical analysis

The samples were crushed in the laboratory of the Regional Geological Mineral Research Institute of Langfang, Hebei Province. The rock samples were first crushed to grains ranging between 2 cm and 4 cm. Subsequently, the grains were cleaned in an ultrasonic bath with 3%–5% dilute HCl solution. Finally, the samples were pulverized to 200 mesh to improve homogeneity. The geochemical analyses were conducted at the Key Laboratory of Western Mineral Resources and Geological Engineering of the Ministry of Education, Chang'an University. The major elements were determined by X-ray fluorescence (XRF) and trace elements, including rare-earth elements (REE), were determined using a ThermoX7 ICP-MS (Fan and Kerrich, 1997). Powder samples (500 mg) were placed into a PTFE crucible with high-purity 1.0 mL HF and 1.5 mL  $\text{HNO}_3$  solutions. Then, the samples were diluted to 50 mL in a centrifuge tube and the final solution was used in the ICP-MS analyses. The precision and accuracy were better than 10%.

### 5 Analytical Results

#### 5.1 Zircon U–Pb geochronology

The zircons in the granodiorite are light yellow to colorless and transparent. The zircon grains in the CL images are relatively euhedral and mostly short and columnar (Fig. 3a). The zircon length ranges from 80 to 110  $\mu\text{m}$ . The obvious oscillatory zoning suggests that the zircon grains are magma-origin. A 30- $\mu\text{m}$  diameter laser spot was used to analyze the zircons in sample XRD050/8. A total of 21 points were measured, with good correspondence between  $^{206}\text{Pb}/^{238}\text{U}$  and  $^{207}\text{Pb}/^{235}\text{U}$  for 20 points (Fig. 3c). The  $^{206}\text{Pb}/^{238}\text{U}$  ages range from  $243\pm 2$  to  $249\pm 1$  Ma (Table 1). The  $^{206}\text{Pb}/^{238}\text{U}$  average weighted age is  $246\pm 0.62$  Ma (MSWD = 1.03). Consequently, the

crystallization age of the granodiorite was most likely intruded in Early Triassic.

Zircons in the MMEs are light yellow to colorless and transparent. The CL images shows euhedral and subhedral zircon grains, most of which are columnar but some are egg-shaped (Fig. 3b). The zircon grain length ranges from 70 to 110  $\mu\text{m}$ . The obvious oscillatory zoning suggests that the zircon grains are magma-origin. Some zircon grains are dark gray in color with obscure annulus. The LA-MC-ICP-MS laser spot size for analyzing the zircons in sample XRD050/10 was 30  $\mu\text{m}$ . A total of 21 points were measured, with good correspondence between  $^{206}\text{Pb}/^{238}\text{U}$  and  $^{207}\text{Pb}/^{235}\text{U}$  for 18 points. The  $^{206}\text{Pb}/^{238}\text{U}$  ages of eight points range from 313 Ma to 1020 Ma. Moreover, some zircons have nearly round shapes. The CL images show patches and embayments (Fig. 3b), which are characteristics of metamorphic zircons (Jian Ping et al., 2001). These zircons were excluded in the age calculations. The  $^{206}\text{Pb}/^{238}\text{U}$  and  $^{207}\text{Pb}/^{235}\text{U}$  ages measured at ten other points show better accordance (Fig. 3d). The corresponding  $^{206}\text{Pb}/^{238}\text{U}$  ages range from  $244\pm 1$  to  $246\pm 1$  Ma (Table 1). The average weighted age of  $^{206}\text{Pb}/^{238}\text{U}$  is  $245.45\pm 0.9$  Ma (MSWD = 0.24). Consequently, the crystallization age of the MME is  $245.45\pm 0.9$  Ma.

#### 5.2 Major elements

The granodiorite has a  $\text{SiO}_2$  content from 60.26 wt% to 65.88 wt%,  $\text{Al}_2\text{O}_3$  from 14.91 wt% to 16.34 wt%, the relatively high  $\text{Na}_2\text{O}$  content from 2.98 wt% to 3.36 wt% (3.15 wt% average), and  $\text{K}_2\text{O}$  content from 1.32 wt% to 3.01 wt% (2.12 wt% average), with  $\text{Na}_2\text{O}/\text{K}_2\text{O}$  varying from 1.06 to 2.42 (1.60 average). The aluminum saturation index ( $A/\text{CNK}$ ) ranges from 0.92 to 0.99 with an average value of 0.94. Figure 4a shows that the  $A/\text{CNK}$  and  $A/\text{NK}$  fall into the metaluminous range. Figure 4b shows that the granodiorite belongs to the medium-K calc-alkaline series. In the TAS diagram, the samples are plotted in the diorite and granodiorite fields (Fig. 4c). The samples are high in  $\text{FeO}^T$  (4.98 wt%–6.62 wt%),  $\text{MgO}$  (1.76 wt%–2.62 wt%), and  $\text{TiO}_2$  (0.55 wt%–0.78 wt%),  $\text{Mg}^{\#}$  (38–42). The Harker diagram (Fig. 5) shows that  $\text{TiO}_2$ ,  $\text{FeO}^T$ ,  $\text{Al}_2\text{O}_3$ ,  $\text{CaO}$ ,  $\text{MgO}$ ,  $\text{P}_2\text{O}_5$  increase and  $\text{K}_2\text{O}$  decrease with increasing  $\text{SiO}_2$ .

The porphyritic diorite is relatively poor in  $\text{SiO}_2$  and  $\text{K}_2\text{O}$  and rich in  $\text{CaO}$ ,  $\text{FeO}^T$ ,  $\text{MgO}$ , and  $\text{TiO}_2$ .  $\text{SiO}_2$  ranges from 50.44 wt% to 55.33 wt%,  $\text{TiO}_2$  from 0.78 wt% to 0.88 wt%,  $\text{Al}_2\text{O}_3$  from 15.61 wt% to 16.38 wt%,  $\text{Na}_2\text{O}$  from 1.98 wt% to 3.44 wt% (2.71% average), and  $\text{K}_2\text{O}$  from 0.75 wt% to 1.14 wt% (0.95 wt% average).  $\text{Na}_2\text{O}/\text{K}_2\text{O}$  varies from 1.74 to 4.59 (3.16 average). The  $A/\text{CNK}$  ranges from 0.76 to 0.85 (0.81 average). In the  $A/\text{CNK}$ – $A/\text{NK}$  diagram (Fig. 4a), the diorite plots on the metaluminous field and in the  $\text{SiO}_2$ – $\text{K}_2\text{O}$  diagram (Fig.

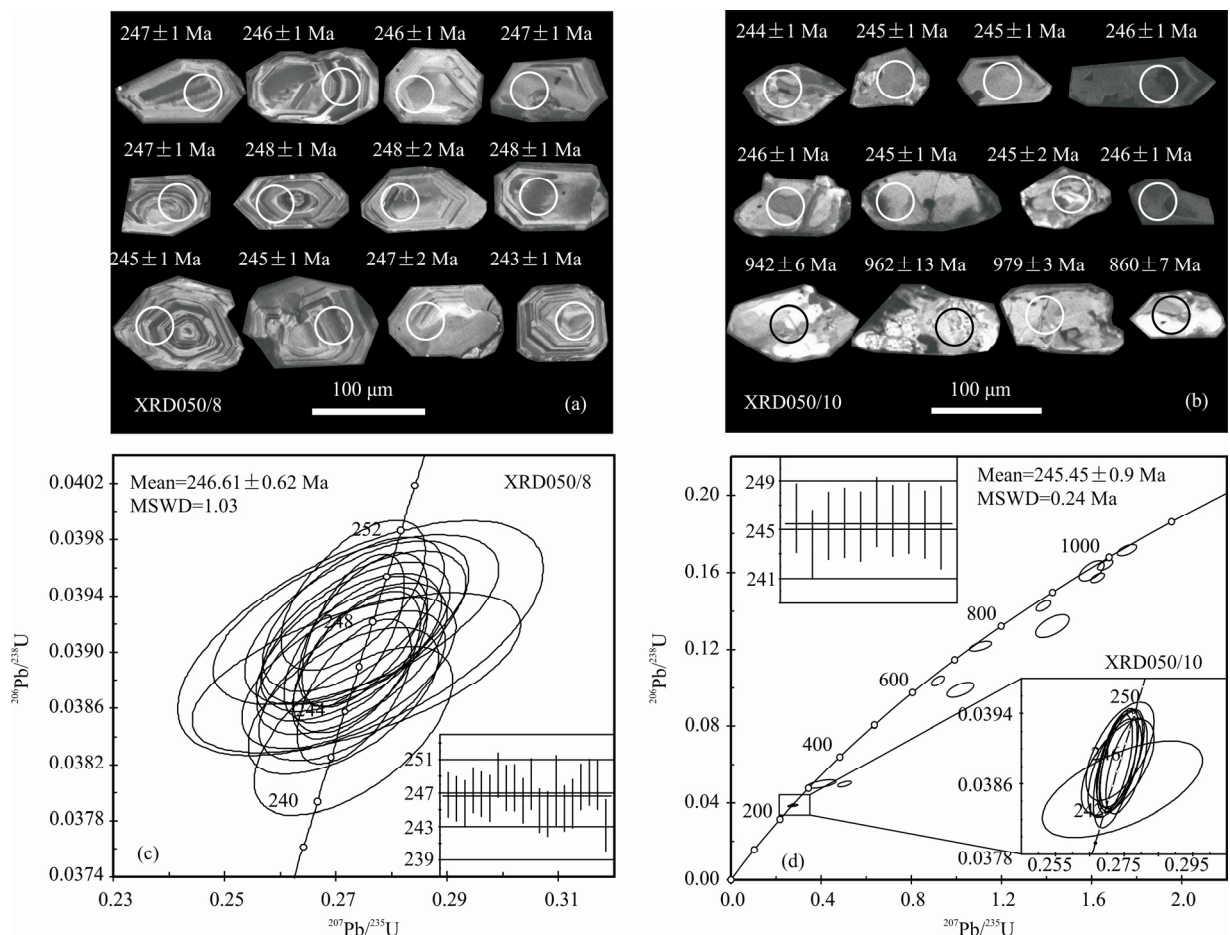


Fig. 3. (a-b) Cathodoluminescence photos of typical single-crystal zircons and their apparent ages(Ma) for the QSG (XRD050/8) and their MME (XRD050/10); (c-d) LA-MC-ICP-MS zircon U–Pb concordant age diagram and weighted histogram for the QSG (XRD050/8) and their MME (XRD050/10).

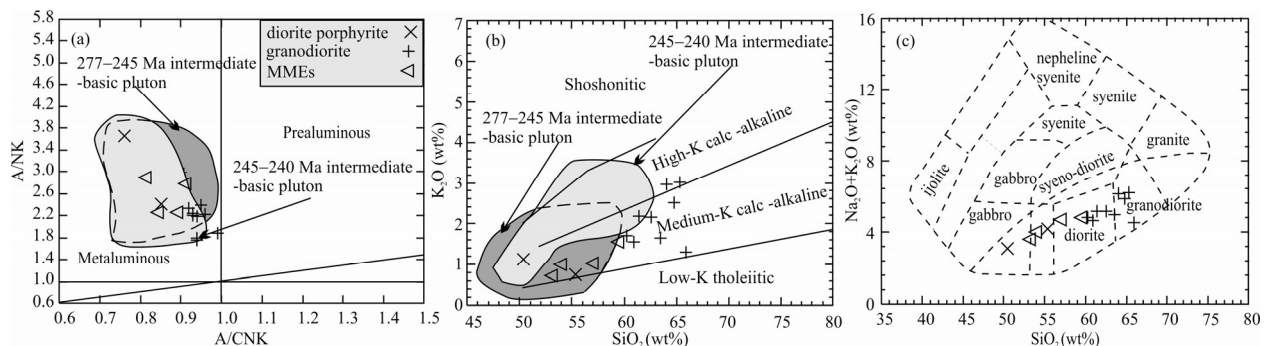


Fig. 4. (a) A/NK–A/CNK diagrams (after Maniar and Piccoli, 1989); (b) K<sub>2</sub>O–SiO<sub>2</sub> diagrams (after Rollinson, 1993); (c) Na<sub>2</sub>O+K<sub>2</sub>O–SiO<sub>2</sub> classifying-naming diagrams (after Wilson, 1989).

Data for 277–245 Ma intermediate-basic pluton are from (Xiong Fuhao et al., 2011; Xiong et al., 2012, 2013, 2014; Huang et al., 2014; Liu et al., 2014); Data for 245–240 Ma intermediate-basic pluton are from (Li Bile et al., 2012; Zhang et al., 2012; Xia et al., 2015b), respectively (the same below).

4b), it plots in the medium-K calc-alkaline series. In the TAS diagram, the samples fall into the gabbro and diorite fields (Fig. 4c). The MgO content ranges from 4.27 wt% to 6.45 wt%, FeO<sup>T</sup> ranges from 8.82 wt% to 9.71 wt%, and Mg<sup>#</sup> ranges from 46 to 54.

The main elemental characteristics of the MMEs are similar to those of the porphyritic diorite but the variations

are greater. SiO<sub>2</sub> ranges from 53.05 wt% to 59.37 wt%, TiO<sub>2</sub> from 0.79 wt% to 1.40 wt%, Al<sub>2</sub>O<sub>3</sub> from 15.97 wt% to 16.71 wt%, Na<sub>2</sub>O from 2.87 wt% to 3.66 wt% (3.20 wt% average), and K<sub>2</sub>O from 0.73 wt% to 1.55 wt% (1.08 wt% average). Na<sub>2</sub>O/K<sub>2</sub>O varies from 2.12 to 3.93. The A/CNK ranges from 0.81 to 0.91 and suggests that the MMEs belong to the metaluminous, medium-K calc-

**Table 1 LA-MC-ICP-MS zircon U-Pb isotope analysis results for the Qu'shiang gneissic pluton (XRD050/8) and their MMEs (XRD050/10) in the eastern part of the EKOB**

Spot no	element content	isotopic ratios and err										apparent age (Ma)						
		Pb (ppm)	U (ppm)	$^{206}\text{Pb}/^{238}\text{U}$	$1\sigma$	$^{207}\text{Pb}/^{235}\text{U}$	$1\sigma$	$^{208}\text{Pb}/^{232}\text{Th}$	$1\sigma$	$^{232}\text{Th}/^{238}\text{U}$	$1\sigma$	$^{206}\text{Pb}/^{238}\text{U}$	$1\sigma$	$^{207}\text{Pb}/^{235}\text{U}$	$1\sigma$	$^{206}\text{Pb}/^{207}\text{Pb}$	$1\sigma$	
Grandiorite (XRD050/8)																		
050/8-01	17	419	0.0390	0.0002	0.2736	0.0053	0.0508	0.0010	0.0089	0.0001	0.7697	0.0036	247	1	246	5	234	45
050/8-02	22	516	0.0389	0.0002	0.2744	0.0049	0.0511	0.0009	0.0093	0.0001	0.8314	0.0010	246	1	246	4	245	40
050/8-03	8	187	0.0389	0.0002	0.2723	0.0079	0.0508	0.0015	0.0092	0.0001	0.6681	0.0024	246	1	245	7	233	66
050/8-04	15	364	0.0391	0.0002	0.2735	0.0069	0.0507	0.0012	0.0121	0.0002	0.5686	0.0014	247	1	245	6	228	55
050/8-05	17	377	0.0390	0.0002	0.2723	0.0068	0.0506	0.0012	0.0128	0.0002	0.7429	0.0016	247	1	245	6	222	55
050/8-06	8	188	0.0390	0.0002	0.2729	0.0070	0.0508	0.0013	0.0134	0.0002	0.5170	0.0032	246	1	245	6	232	59
050/8-07	11	258	0.0394	0.0002	0.2731	0.0053	0.0503	0.0009	0.0171	0.0002	0.5199	0.0010	249	1	245	5	207	44
050/8-08	17	382	0.0392	0.0002	0.2731	0.0038	0.0506	0.0007	0.0155	0.0001	0.6755	0.0030	248	1	245	3	222	32
050/8-09	15	319	0.0392	0.0002	0.2748	0.0047	0.0509	0.0008	0.0205	0.0002	0.6838	0.0025	248	1	247	4	237	36
050/8-10	17	402	0.0389	0.0002	0.2737	0.0047	0.0510	0.0009	0.0125	0.0001	0.6777	0.0007	246	1	246	4	242	39
050/8-11	7	160	0.0392	0.0002	0.2735	0.0105	0.0506	0.0019	0.0141	0.0001	0.6230	0.0006	248	2	246	9	221	88
050/8-12	18	424	0.0387	0.0002	0.2733	0.0042	0.0512	0.0008	0.0114	0.0000	0.8351	0.0015	245	1	245	4	249	35
050/8-13	13	302	0.0387	0.0002	0.2713	0.0070	0.0509	0.0012	0.0126	0.0002	0.6015	0.0009	244	1	244	6	237	56
050/8-14	8	178	0.0391	0.0003	0.2744	0.0134	0.0509	0.0024	0.0148	0.0003	0.5564	0.0014	247	2	246	12	236	107
050/8-15	10	233	0.0388	0.0002	0.2728	0.0068	0.0511	0.0013	0.0112	0.0001	0.6911	0.0007	245	6	243	58		
050/8-16	10	243	0.0389	0.0002	0.2737	0.0121	0.0511	0.0022	0.0116	0.0001	0.5444	0.0011	246	1	245	11	245	101
050/8-17	8	191	0.0392	0.0002	0.2749	0.0075	0.0509	0.0014	0.0137	0.0001	0.5595	0.0015	248	1	247	7	236	62
050/8-18	11	251	0.0393	0.0002	0.2732	0.0067	0.0505	0.0012	0.0166	0.0003	0.5191	0.0004	248	1	245	6	216	53
050/8-19	15	315	0.0392	0.0002	0.2737	0.0082	0.0506	0.0014	0.0158	0.0003	0.8177	0.0005	248	1	246	7	224	62
050/8-20	12	219	0.0458	0.0004	0.5924	0.0168	0.0937	0.0022	0.0230	0.0007	0.4996	0.0094	289	2	472	13	1502	45
050/8-21	12	258	0.0384	0.0002	0.2731	0.0073	0.0515	0.0013	0.0208	0.0003	0.5930	0.0004	243	2	245	7	264	57
MMEs (XRD050/10)																		
050/10-01	3	65	0.0498	0.0009	0.4021	0.0262	0.0586	0.0038	0.0819	0.0061	0.0334	0.0013	313	6	343	22	551	143
050/10-02	61	1474	0.0389	0.0002	0.2739	0.0028	0.0511	0.0005	0.0156	0.0002	0.4303	0.0032	246	3	245	22		
050/10-03	31	743	0.0385	0.0002	0.2745	0.0095	0.0517	0.0018	0.0174	0.0001	0.3964	0.0007	244	1	246	9	270	80
050/10-04	45	260	0.1573	0.0010	1.6265	0.0127	0.0750	0.0006	0.0452	0.0002	0.7222	0.0043	942	6	981	8	1068	15
050/10-05	22	130	0.1609	0.0022	1.6001	0.0228	0.0721	0.0007	0.0507	0.0007	0.4128	0.0190	962	13	970	14	989	19
050/10-06	54	295	0.1640	0.0011	1.6603	0.0140	0.0734	0.0006	0.0451	0.0001	0.7362	0.0034	979	7	994	8	1026	17
050/10-07	36	194	0.1714	0.0012	1.7569	0.0176	0.0743	0.0008	0.0428	0.0002	0.7500	0.0064	1020	7	1030	10	1050	21
050/10-08	29	262	0.1037	0.0011	0.9183	0.0118	0.0643	0.0006	0.0378	0.0001	0.4283	0.0063	636	7	661	8	750	21
050/10-09	25	193	0.1217	0.0010	1.1070	0.0201	0.0659	0.0010	0.0410	0.0003	0.4226	0.0036	741	6	757	14	805	32
050/10-10	67	1643	0.0388	0.0002	0.2731	0.0043	0.0511	0.0008	0.0143	0.0002	0.4411	0.0042	245	4	244	36		
050/10-11	72	1811	0.0388	0.0002	0.2723	0.0021	0.0509	0.0004	0.0095	0.0000	0.5378	0.0009	246	1	245	2	235	18
050/10-12	38	972	0.0388	0.0002	0.2723	0.0032	0.0515	0.0005	0.0120	0.0001	0.3978	0.0039	245	1	245	3	237	24
050/10-13	30	765	0.0390	0.0002	0.2738	0.0040	0.0510	0.0007	0.0116	0.0001	0.3198	0.0030	246	1	245	4	239	32
050/10-14	17	125	0.1322	0.0024	1.4262	0.0304	0.0783	0.0009	0.0524	0.0010	0.2194	0.0138	800	15	900	19	1153	22
050/10-15	57	1381	0.0389	0.0002	0.2741	0.0026	0.0512	0.0005	0.0112	0.0001	0.5814	0.0040	246	1	246	2	248	24
050/10-16	42	1145	0.0389	0.0002	0.2736	0.0023	0.0510	0.0004	0.0184	0.0003	0.1026	0.0017	246	2	246	2	242	19
050/10-17	56	1404	0.0388	0.0002	0.2757	0.0025	0.0515	0.0005	0.0108	0.0000	0.5339	0.0014	245	1	247	2	264	20
050/10-18	33	214	0.1428	0.0011	1.3858	0.0133	0.0704	0.0007	0.0527	0.0003	0.4327	0.0040	860	7	883	9	940	20
050/10-19	12	112	0.0990	0.0016	1.0179	0.0244	0.0746	0.0016	0.0534	0.0009	0.2645	0.0096	608	10	713	17	1058	43
050/10-20	8	172	0.0498	0.0006	0.5038	0.0127	0.0734	0.0023	0.2171	0.0137	0.0316	0.0002	313	4	414	10	1024	63
050/10-21	33	836	0.0388	0.0003	0.2724	0.0026	0.0510	0.0006	0.0126	0.0001	0.3907	0.0046	245	2	245	2	239	25

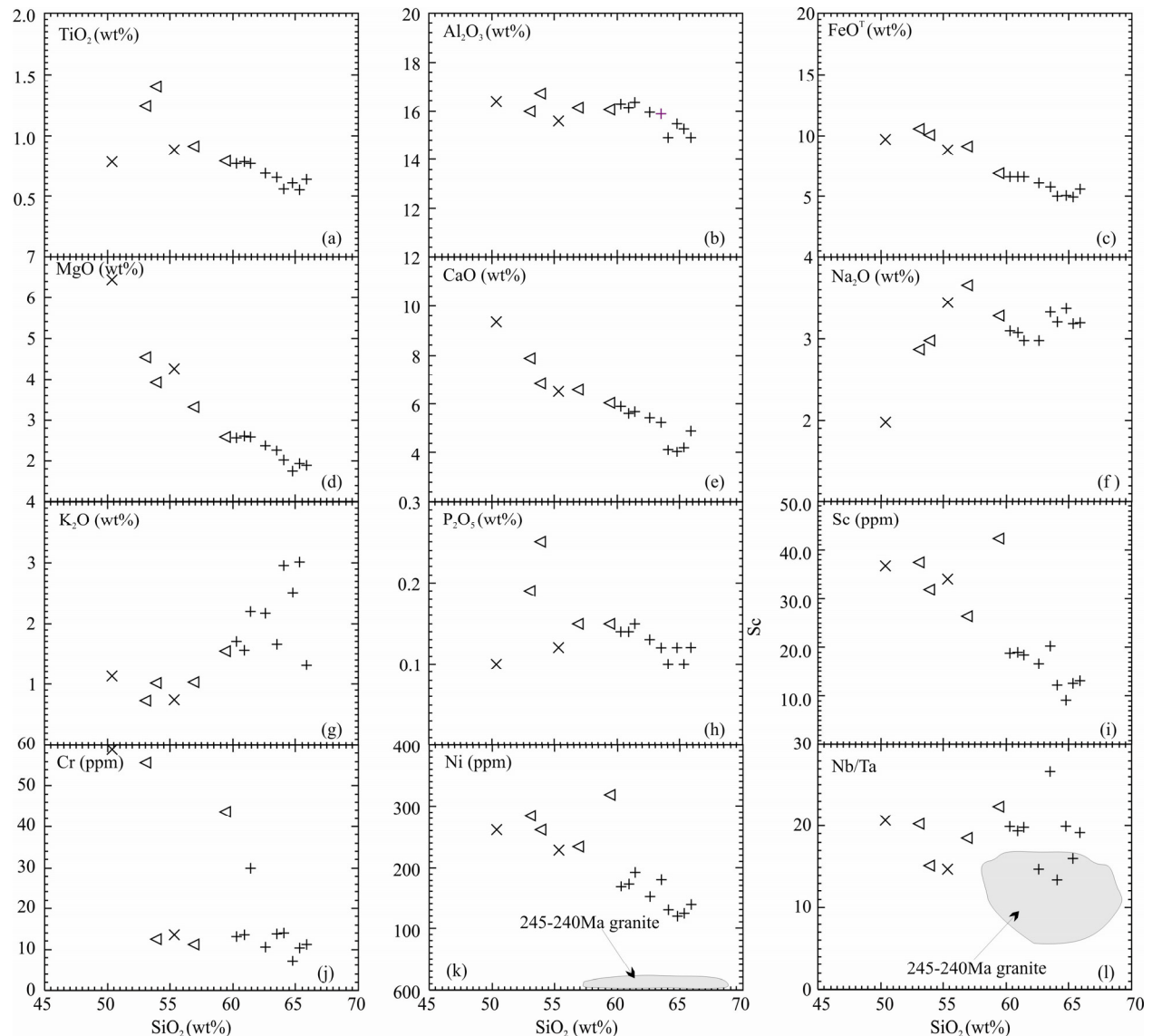


Fig. 5. Harker diagrams for the QSG. Symbols are as in Fig.4.

Data for 245–240Ma granite are form (Chen Hongwei et al., 2005; Wang Song et al., 2009; Zhang et al., 2012; Xiong et al., 2014; Li et al., 2015; Xia et al., 2015b), respectively (the same below).

alkaline series (Fig. 4a and 4b). The samples fall into the gabbro and diorite fields in the TAS diagram (Fig. 4c). The MgO content ranges from 2.60 wt% to 5.54 wt%, FeO<sup>T</sup> is from 6.88 wt% to 10.59 wt%, and Mg<sup>#</sup> ranges from 40 to 43.

### 5.3 Rare-earth elements (REE)

The granodiorite is enriched in REE (113.52 ppm to 226.02 ppm), with La/Yb<sub>N</sub> ranging from 9.11 to 22.94 (12.76 average). The chondrite-normalized REE distribution shows strong LREE enrichment and HREE depletion (Fig. 6a). The Yb ranges from 1.38 ppm to 1.92 ppm and Lu ranges from 0.26 ppm to 0.30 ppm. Yb/Lu (5.40–6.37) and Gd/Yb<sub>N</sub> (1.98–2.16) suggest a flat HREE distribution model. The Eu/Eu<sup>\*</sup> ranges from 0.47 to 0.50, suggesting negative Eu anomaly.

The porphyritic diorite has total REE content of 69.70 ppm–87.74 ppm and is lower than that of the granodiorite. La/Yb<sub>N</sub> ranges from 5.72 to 10.43 (8.04 average). The distribution pattern of REE is similar to that of granodiorite, but the fractionation of REE is slightly lower (Fig. 6a). The Yb content ranges from 1.16 ppm to 1.26 ppm, Lu ranges from 0.18 ppm to 0.20 ppm, Yb/Lu ranges from 6.24 ppm to 6.38, and Gd/Yb<sub>N</sub> ranges from 2.35 to 2.36. The Eu/Eu<sup>\*</sup> is from 0.45 to 0.58 and suggests negative Eu anomaly.

The MME has total REE content that ranges from 92.45 ppm to 148.90 ppm, average is 117.45 ppm, and is between that of the granodiorite and the porphyritic diorite. La/Yb<sub>N</sub> ranges from 2.56 to 9.62 (7.37 average). Yb/Lu ranges from 5.99 to 6.46 and Gd/Yb<sub>N</sub> ranges from 1.96 to 2.66. The Eu/Eu<sup>\*</sup> ranges from 0.45 to 0.58 and

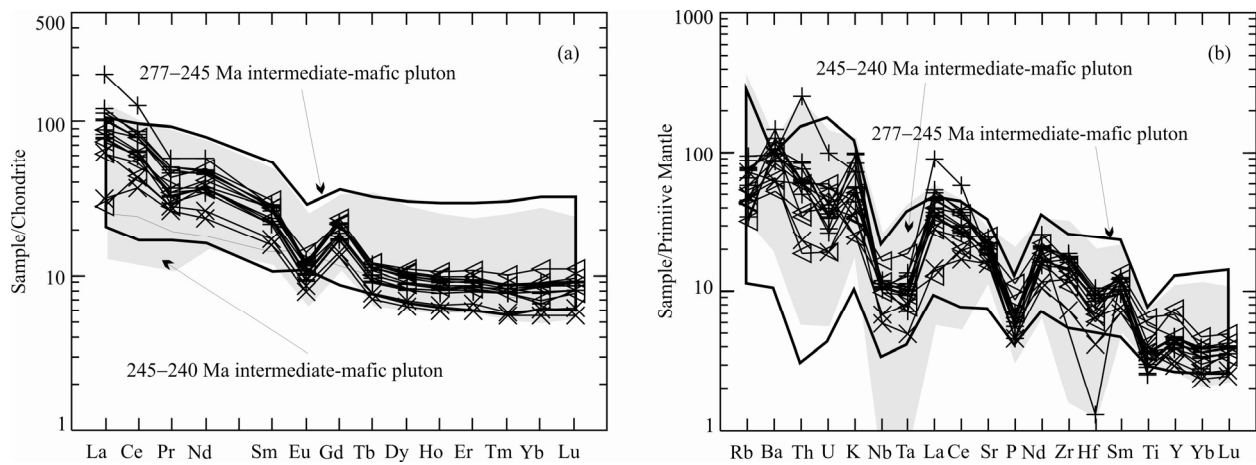


Fig. 6. (a) Chondrite-normalized REE distribution patterns (normalization values after Boynton, 1984) and (b) primitive mantle-normalized trace element spider diagrams (normalization values after Sun and McDonough, 1989) for the QSG. Symbols are as in Fig.4.

suggests negative Eu anomaly.

#### 5.4 Trace elements

Figure 6b shows a primitive mantle-normalized trace-element spider diagram. The granodiorite is enriched in large-ion lithophile elements (LILE), including Rb, Th, Ba, and Cs, and is depleted in high-field strength elements (HFSE), including Nb, Ta, and Ti. The Rb content ranges from 21.88 ppm to 61.12 ppm, Sr content ranges from 349.77 ppm to 518.11 ppm, and Y content ranges from 17.51 ppm to 21.12 ppm. Rb/Sr ranges from 0.06 to 0.17 (0.11 average) and Sr/Y from 18.87 to 25.52 (21.56 average). The Nb content ranges from 7.39 ppm to 8.42 ppm and Ta from 0.29 ppm to 0.55 ppm. Nb/Ta ranges from 13.38 to 28.88 (18.81 average). The Cr content ranges from 7.22 ppm to 29.96 ppm (13.76 ppm average). The Ni content is relatively high and ranges from 120.45 ppm to 191.65 ppm (153.59 ppm average).

The trace element content of the porphyritic diorite is similar to that of the granodiorite but with lower LILE (Fig. 6b). The Sr content ranges from 330.49 ppm to 481.36 ppm and Y from 13.12 ppm to 14.37 ppm. Sr/Y ranges from 25.18 to 33.50. The Nb content ranges from 4.13 ppm to 4.83 ppm and Ta from 0.22 ppm to 0.33 ppm. Nb/Ta ranges from 14.56 to 22.51 (average 17.52). The Ni and Cr contents of the porphyritic diorite are higher than those of the granodiorite. Cr ranges from 13.35 ppm to 59.01 ppm (average 36.25 ppm). Ni ranges from 228.53 ppm to 261.29 ppm (average 244.91 ppm).

The trace element content of the MMEs is similar to that of the porphyritic diorite but with larger range. The Sr content ranges from 324.23 ppm to 531.10 ppm and Y from 17.82 ppm to 33.94 ppm. Sr/Y ranges from 9.55 to 29.81. The Nb content ranges from 6.93 ppm to 11.65 ppm and Ta from 0.31 ppm to 0.77 ppm. Nb/Ta ranges

from 15.13 to 22.51 (average 19.07). The Ni and Cr contents of the MME are similar to those of the porphyritic diorite. The Cr content ranges from 11.30 ppm to 55.62 ppm (average 30.77 ppm). The Ni content ranges from 233.89 ppm to 318.49 ppm (average 274.38 ppm).

## 6 Discussion

### 6.1 Petrogenesis of the porphyritic diorite

The average Ti/Yb ratio of the porphyritic diorite (4016) is similar to that of magmas without crustal contamination (5000; Hart, 1986). Moreover, the average Nb/Ta ratio of the magma (17.52) is similar to that of the primitive mantle (17.78; Sun and McDonough, 1989; Weyer et al., 2003), suggesting that the porphyritic diorite is relatively less contaminated by continental crust materials (Wedepohl, 1995). The porphyritic diorite has low SiO<sub>2</sub>, high Cr and Ni content, high Mg<sup>#</sup> (46–54) and Nb/Ta ratio, suggesting a possible mantle origin (Rapp and Watson, 1995). Moreover, their enrichment in LILE and depletion in HFSE are similar to that of the Middle Permian–Early Triassic intermediate–basic magmatic rocks of the EKOB (Fig. 6b), hinting toward an enriched magma source modified by subduction metasomatic fluids (McCulloch and Gamble, 1991; Luhr and Haldar, 2006; Zhao et al., 2007). The Th/Ta–La/Yb diagram introduced by Condie (2002) is useful in constraining the tectonic setting of basalts. The high Th/Ta and La/Yb values in the porphyritic diorite (Fig. 7) support subduction origin with upper crust and enriched mantle rather than depleted mantle-recycling slab characteristics, further suggesting that subduction fluids modified the magma source region. The high Th/Yb and Nb/Yb values in the porphyritic diorite (Fig. 8a) support a mantle source between E-MORB and OIB. These characteristics suggest that the magma source region may

**Table 2 Major (wt%) and trace element (ppm) analysis results for the Qu'shiang gneissic pluton and their MMEs in eastern part of the EKOB**

sample no.	XRD05/03	XRD05/05	XRD05/06	XRD05/08	XRD05/09	XRD05/10	XRD05/11	XRD05/12	XRD05/13	XRD05/21	XRD05/22	XRD05/23	XRD05/24	XRD05/25	XRD05/26
lithology	granodiorite	MMEs	granodiorite	diorite porphyrite	granodiorite	diorite porphyrite	granodiorite								
SiO <sub>2</sub>	64.77	63.51	59.37	64.05	53.88	53.05	65.33	56.88	65.88	62.58	61.40	50.40	55.33	60.94	60.26
TiO <sub>2</sub>	0.61	0.65	0.79	0.56	1.40	1.24	0.55	0.91	0.64	0.69	0.77	0.78	0.88	0.78	0.77
Al <sub>2</sub> O <sub>3</sub>	15.48	15.89	16.06	14.91	16.71	15.97	15.28	16.12	14.91	15.95	16.34	16.38	15.61	16.14	16.26
FeO <sup>f</sup>	5.12	5.75	6.88	5.04	10.01	10.53	4.98	9.09	5.60	6.13	6.59	9.71	8.82	6.62	6.57
MnO	0.09	0.10	0.12	0.08	0.19	0.21	0.09	0.21	0.09	0.11	0.18	0.14	0.11	0.11	0.11
MgO	1.76	2.25	2.60	2.01	3.93	4.54	1.93	3.33	1.89	2.37	2.59	6.45	4.27	2.62	2.58
CaO	4.05	5.27	6.04	4.11	6.85	7.87	4.23	6.59	4.89	5.46	5.71	9.34	6.53	5.63	5.92
Na <sub>2</sub> O	3.36	3.32	3.28	3.20	2.98	2.87	3.18	3.66	3.19	2.98	2.98	1.98	3.44	3.08	3.10
K <sub>2</sub> O	2.51	1.67	1.55	2.95	1.02	0.73	3.01	1.03	1.32	2.17	2.19	1.14	0.75	1.56	1.71
P <sub>2</sub> O <sub>5</sub>	0.12	0.12	0.15	0.10	0.25	0.19	0.10	0.15	0.12	0.15	0.15	0.10	0.12	0.14	0.14
Be	1.31	1.57	1.09	1.42	1.83	2.29	1.29	1.58	1.72	1.37	1.45	1.05	1.13	1.70	1.62
Sc	9.23	20.21	42.33	12.17	31.97	37.53	12.55	26.29	13.02	16.61	18.54	36.77	34.02	18.96	18.90
V	100.84	148.99	382.70	113.73	308.18	328.20	109.82	199.67	109.87	138.99	154.47	262.38	252.34	152.68	153.66
Cr	7.22	13.73	43.72	13.96	12.46	55.62	10.28	11.30	11.24	10.63	29.96	59.01	13.50	13.64	13.18
Co	7.46	10.64	28.71	8.23	17.97	19.02	7.94	13.13	8.00	10.00	11.18	35.52	20.96	10.99	10.93
Ni	120.45	180.63	318.49	130.57	261.06	284.07	124.42	233.89	138.99	152.47	191.65	261.29	228.53	173.91	169.24
Ga	18.90	22.25	21.74	18.08	23.56	22.27	18.80	21.08	19.85	22.23	22.28	18.35	19.02	21.97	22.49
Rb	41.73	47.00	33.91	47.84	27.83	20.15	61.12	27.29	21.88	49.19	56.09	45.89	31.26	28.48	36.73
Sr	425.71	518.11	531.10	382.43	408.77	349.77	324.23	383.12	392.22	440.22	330.49	481.36	470.35	423.74	
Y	18.04	20.31	17.82	17.51	30.51	21.36	18.53	33.94	18.97	19.37	20.57	13.12	14.37	21.12	21.04
Nb	7.56	7.73	6.93	7.40	11.65	8.29	7.39	7.01	8.42	7.68	7.71	4.13	4.85	8.12	8.14
Cd	0.15	0.05	0.20	0.13	0.17	0.19	0.13	0.20	0.17	0.16	0.15	0.15	0.15	0.17	0.17
In	0.04	0.05	0.06	0.04	0.07	0.11	0.04	0.11	0.04	0.04	0.04	0.05	0.04	0.04	0.04
Cs	1.41	0.97	2.47	0.50	1.39	0.32	0.46	0.44	0.92	1.54	0.99	0.98	0.51	0.84	0.88
Ba	1039.05	841.23	453.59	746.01	584.72	766.55	675.65	369.68	696.82	698.04	599.45	438.49	433.33	895.45	619.81
La	23.68	32.21	19.19	27.46	27.39	22.70	24.37	8.72	25.56	61.64	35.08	9.88	19.51	31.15	37.24
Ce	47.19	63.58	43.36	52.57	64.22	49.20	47.82	35.82	50.99	102.32	70.17	29.57	35.06	63.14	66.79
Pr	4.51	5.65	4.24	4.04	5.24	4.20	3.63	3.42	3.96	7.04	6.21	3.21	3.42	5.93	6.15
Nd	21.93	27.71	21.46	21.99	29.77	24.96	20.56	22.59	22.33	34.68	28.76	14.33	15.91	26.85	28.36
Sm	4.45	5.61	4.60	4.23	6.02	5.37	4.22	5.38	4.57	5.57	5.42	3.10	3.41	5.20	5.49
Eu	0.75	0.92	0.85	0.70	0.90	1.04	0.68	0.88	0.77	0.85	0.89	0.59	0.64	0.88	0.89
Gd	4.73	5.74	4.85	5.53	6.10	5.70	4.42	5.57	4.88	5.64	5.65	3.41	3.68	5.65	5.70
Tb	0.46	0.56	0.48	0.43	0.58	0.57	0.44	0.58	0.51	0.54	0.34	0.37	0.54	0.54	0.54
Hf	2.86	0.40	1.84	2.73	2.57	2.08	2.63	2.32	3.23	2.87	2.97	1.26	1.99	2.97	3.08
Dy	2.70	3.24	2.86	2.60	3.39	3.33	2.68	3.55	2.89	2.95	3.10	2.06	2.25	3.23	
Ho	0.58	0.67	0.61	0.56	0.71	0.70	0.58	0.76	0.60	0.62	0.66	0.43	0.47	0.69	0.68
Er	1.71	1.92	1.74	1.66	2.07	2.01	1.78	2.28	1.81	1.84	1.94	1.26	1.39	2.00	2.00
Tm	0.25	0.27	0.25	0.25	0.28	0.27	0.33	0.26	0.26	0.28	0.18	0.19	0.29	0.28	
Yb	1.38	1.62	1.47	1.66	1.92	1.80	2.30	1.79	1.81	1.87	1.16	1.26	1.92	1.87	
Lu	0.26	0.26	0.25	0.26	0.31	0.28	0.29	0.36	0.28	0.28	0.30	0.18	0.20	0.30	
Ta	0.38	0.29	0.31	0.55	0.77	0.41	0.46	0.38	0.44	0.52	0.39	0.20	0.33	0.42	0.41
Pb	7.51	7.99	4.63	12.40	6.10	6.39	12.26	7.65	8.92	9.23	8.73	4.60	6.70	8.90	8.19
Bi	0.02	0.02	0.02	0.04	0.02	0.03	0.02	0.02	0.02	0.02	0.02	0.03	0.03	0.06	0.02
Th	4.27	5.24	5.24	7.13	5.04	5.08	3.19	5.47	21.55	7.39	1.98	5.06	5.36	6.42	
U	0.77	0.55	0.40	0.89	1.26	1.08	0.59	0.84	1.16	2.10	0.70	0.40	0.92	0.76	
Zr	187.61	8.26	121.70	162.34	170.83	140.06	163.72	152.99	208.05	178.49	194.11	81.97	135.44	187.74	198.75
Mg <sup>#</sup>	37.98	41.08	40.24	41.54	41.16	43.44	40.84	39.49	37.55	40.79	41.18	54.20	46.31	41.35	41.16
δEu	0.50	0.49	0.55	0.49	0.45	0.58	0.48	0.49	0.50	0.47	0.49	0.56	0.55	0.50	0.49
Nb/Ta	19.90	26.88	22.51	13.38	15.13	20.07	16.03	18.57	19.32	14.90	20.47	14.56	19.13	19.80	
Sr/Y	23.59	25.52	29.81	21.84	13.40	18.95	18.87	9.55	20.20	21.40	25.18	33.50	22.27	20.14	
La/Yb	17.16	19.88	13.06	16.57	14.27	12.59	13.51	3.80	14.30	34.02	18.72	8.49	15.47	16.26	

Mg<sup>#</sup> = 100 × (Mg<sup>2+</sup>/(Mg<sup>2+</sup>+TFe<sup>2+</sup>)); Eu/Eu\* = Eu/(Eu/(Sm<sub>N</sub> × Gd<sub>N</sub>))<sup>1/2</sup>

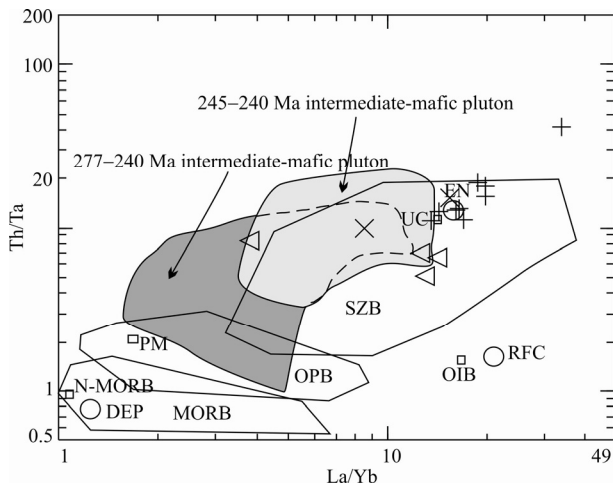


Fig. 7. (a) Th/Ta-La/Yb diagrams for the QSG. Symbols are as in Fig.4.

DEP, depleted mantle; EN, enriched mantle components; MORB, ocean ridge basalt; N-MORB, ocean ridge basalt; OIB, oceanic island basalt; OPB, oceanic plateau basalt; PM, primitive mantle; RFC, recycled slab component; SZB, subduction zone Basalt; UC, upper continental crust. After Condie (2002).

have been in the lithospheric mantle that was modified by subduction metasomatic fluids. The Sm/Yb-Sm plot (Fig. 8b) suggests that the porphyritic diorite is close to the garnet lherzolite partial melting curve, suggesting that the magma formed at depth of lithospheric mantle (Johnson, 1994; Aldanmaz et al., 2000).

## 6.2 Petrogenesis of the granodiorite

The granodiorite is high in amphibole and  $\text{Al}_2\text{O}_3$  and low in  $\text{SiO}_2$ . Therefore, it belongs to the metaluminous, medium-K calc-alkaline series, with low  $\text{P}_2\text{O}_5$  content that negatively correlates with the  $\text{SiO}_2$  content (Fig. 5h).

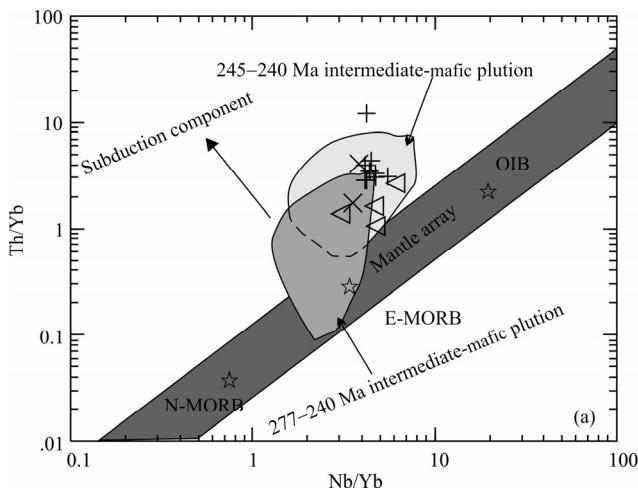


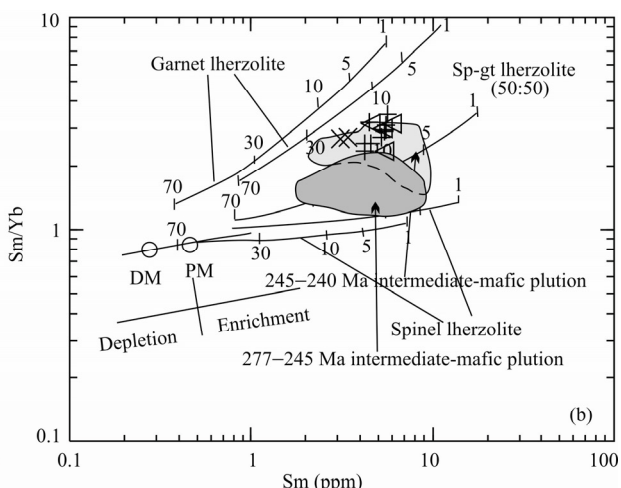
Fig. 8. (a) Th/Yb-Nb/Yb (after Pearce, 2008) and (b) Sm/Yb-Sm (after Zhao and Zhou, 2007) diagrams for the QSG. Symbols are as in Fig.4.

Melt curves are drawn for spinel-lherzolite (with mode and melt mode of  $\text{ol}_{0.530} + \text{opx}_{0.270} + \text{cpx}_{0.170} + \text{sp}_{0.030}$  and  $\text{ol}_{0.060} + \text{opx}_{0.280} + \text{cpx}_{0.670} + \text{sp}_{0.110}$ ; Kinzler, 1997) and for garnet-lherzolite (with mode and melt mode of  $\text{ol}_{0.600} + \text{opx}_{0.200} + \text{cpx}_{0.100}$  and  $\text{ol}_{0.030} + \text{opx}_{0.160} + \text{cpx}_{0.880} + \text{gt}_{0.090}$ ; respectively; Walter, 1998). Mineral/matrix partition coefficients and DMM are from the compilation of McKenzie and O’Nions (1991); primitive mantle, N-MORB and E-MORB compositions are from Sun and McDonough (1989). Tick marks on each curve (or line) correspond to degrees of partial melting for a given mantle source.

These results suggest that it has I-type granitoids characteristics (Li et al., 2007; Wu Fuyuan et al., 2007). The granodiorite is enriched in LILE and depleted in HFSE (Fig. 6a), which are typical characteristics of rocks related to island-arc magmas, and has low Y and Yb, high Sr, and high La/Yb and Sr/Y that are similar to adakitic rocks (Martin, 1999). However, the Y content in the QSG (19.50 ppm average) is slightly higher than that in adakitic rocks (18.00 ppm average). Sr/Y (21.56 average) and La/Yb (18.93 average) are lower in the QSG than in adakitic rocks (40 and 20, respectively) (Defant and Drummond, 1990; Moyen, 2009). Figure 9 shows Sr/Y-Y and La/Yb<sub>N</sub>-Yb<sub>N</sub> diagrams. The samples fall into the transitional field between adakites and island-arc magmas and are closer to the latter. Furthermore, Nb/Ta (18.81 average) and Ni (153.59 ppm average) are obviously higher than in contemporaneous granitic rocks (Fig. 5k and 5l) and oceanic crustal basalts (Li Ruibao et al., 2015). The granodiorite has the characteristics of mantle-derived magma and is not related to granites that are produced by mafic magma underplating in the lower crust (Chen Hongwei et al., 2005; Zhang et al., 2012; Xia et al., 2015b). Figure 10 shows the Zr/Sm-Th/La diagram. Neither magma mixing characteristics are seen (Langmuir et al., 1978). The QSG has similar crystallization age as the MMEs and similar mineral compositions and trace elements as the porphyritic diorite. In particular, it has high Nb/Ta, Cr, and Ni, suggesting that the QSG and porphyritic diorite evolved in the same magma chamber.

## 6.3 Petrogenesis of the MME

The MMEs are usually elliptical, with typical magmatic



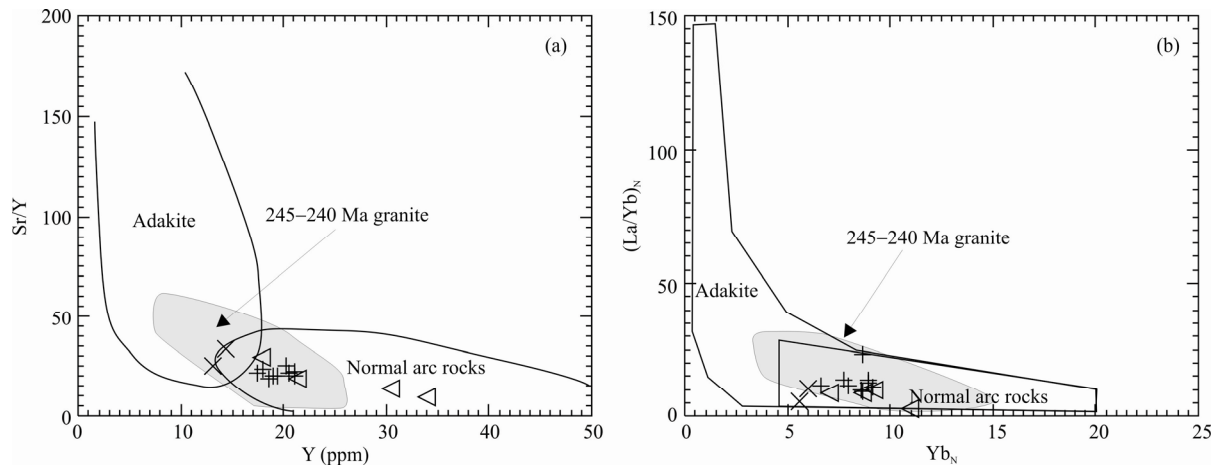


Fig. 9. (a) Sr/Y-Y and (b)(La/Yb)N-Yb<sub>N</sub> diagrams for the QSG (after Castillo, 2008). Symbols are as in Fig.4.

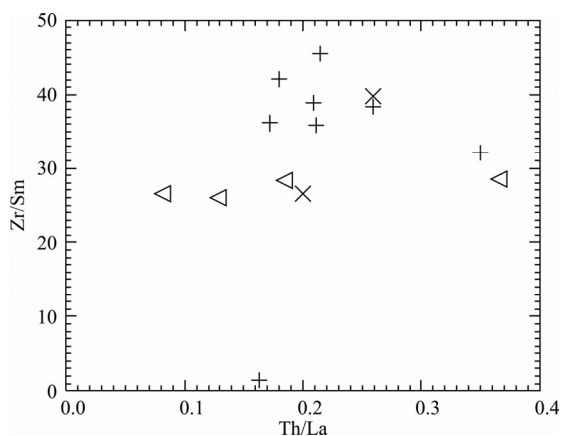


Fig. 10. Zr/Sn-Th/La diagram for the QSG.

textures and structures (Fig. 2a–b, and e), and have similar crystallization age as the host rocks, suggesting that they are not residual bodies or wall rocks (White et al., 1999). In a Harker diagram (Fig. 5), the trends and element contents and ratios of MMEs are between those of porphyritic diorite and granodiorite. They also have similar REE distribution patterns and spider diagrams. The above suggest that the MMEs are products of the mixing of mafic and granodioritic magmas (Dahlquist, 2002; Donaire et al., 2005). However, the mafic magma probably had evolved before mixing with the granodioritic magma.

The above suggest that subduction-induced partial melting of the mantle produced primitive magmas. Subsequently, the magmas after early crystal fractionation ascended into the lower crust (such as the Kuhai Group) and formed the granodiorite. Then, mafic magmas intruded into the granodioritic magma and formed the MMEs and porphyritic diorite. The gneissic structure developed because of ductile shearing.

#### 6.4 Tectonic setting

The granodiorite has a crystallization age of 246.61±

0.62 Ma and geochemical characteristics of island-arc magmatic rocks. In tectonic setting discrimination diagrams (Fig. 11), the QSG samples are similar to most magmatic rocks of similar age and fall into the island-arc magmas field. Consequently, the QSG is considered to be the product of partial melt mantle owing to the northward subduction of the Buqingshan–A'nyemaqen oceanic crust. There are many granitic rocks of 277 Ma–240 Ma, including many MMEs with the characteristics of island-arc magmatic rocks (Yuan Wanming et al., 2000; Sun Yu et al., 2009; Feng Chengyou et al., 2012; Dai et al., 2013; Li Zuochen et al., 2013; Chen Guochao, 2014; Liu et al., 2014; Luo Mingfei et al., 2014, 2015; Xia et al., 2014, 2015a; Chen et al., 2015; Li et al., 2015). However, the period of 240 Ma–230 Ma is devoid of magmatism in the area and syncollisional intrusive rocks are scarce (Zhang et al., 2012; Xia Rui et al., 2014; Xiong et al., 2014; Chen Guochao and Pei Xianzhi, to be published). Xia et al. (2015b) investigated the Nange Beach pluton in the EKOB and confirmed that it represents the late-stage subduction in Early Triassic and that the Buqingshan–A'nyemaqen oceanic crust closed around 243 Ma.

Sedimentological studies suggest that the Early Triassic Hongshuichuan Formation belongs to a forearc basin depositional system. The deposits reflect the northward subduction of the Buqingshan–A'nyemaqen Ocean and confirm that the EKOB was undergone subduction in Early Triassic (Li Ruibao et al., 2012). Furthermore, metamorphic geochronology studies suggest that tectono-metamorphism related to subduction around 246 Ma in the EKOB (Chen Nengsong et al., 2007). Therefore, these investigations suggest that the EKOB in Early Triassic was part of the subduction of the Buqingshan–A'nyemaqen Ocean.

The Central East Kunlun ophiolitic melange belt is a multiply cycled collisional belt (Wang Guocan et al., 1999; Wu Zhenhan et al., 2007; Lu Lu et al., 2010; Zhang

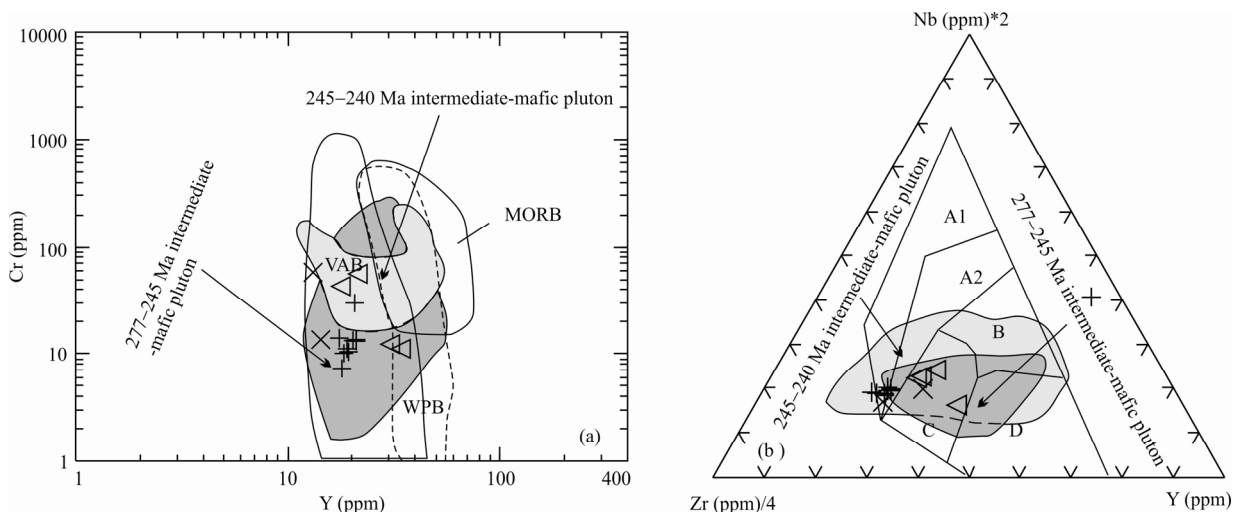


Fig. 11. (a) Cr-Y (after Pearce, 1982) and (b) Nb-Zr-Y (after Mullen, 1986) diagrams for the QSG. Symbols are as in Fig. 4. A1: within-plate alkali basalts; A2: with-plate alkali basalts and within-plate tholeiites; B: E-type MORB; C: within-plate tholeiites and volcanic-arc basalts; D: N-type MORB and volcanic-arc basalts.

Zicheng et al., 2010). The QSG is part of the belt and has gneissic structures because of a late ductile and strike-slip shearing. The strike-slip shearing of the Central East Kunlun fault was part of the Paleo-Tethyan evolution and is younger than 246 Ma. Thus, the Buqingshan-A'nyemaqen Ocean had not closed in middle Early Triassic.

## 6.5 Multistage magmatic activity in the EKOB in the Middle Permian–Early Triassic subduction

A large amount of magmatic rocks intruded the EKOB during 277 Ma–240 Ma into two stages (Fig. 12). The magmatic rocks in both stages display characteristics similar to island-arc magmas despite the differences between them.

The duration of magmatism in the 277 Ma–245 Ma stage

was longer than the 245 Ma–240 Ma stage and became more intense with time and peaking around 250 Ma. The main bodies of the pluton belong to the metaluminous, medium-K calc-alkaline series and are characterized by weak fractionation between HREEs and LREEs. The rocks are enriched in LILE and depleted in HFSE with a relatively concentrated distribution (Fig. 6). The duration of magmatism in the 245 Ma–240 Ma stage is relatively short but intense. The rocks of this stage are widespread (Fig. 12) and transitional between the metaluminous and medium-K calc-alkali series and high-K calc-alkali series (Fig. 4a and 4b). The corresponding REE and trace elements are identical to those from the early stage. However, the fractionation of HREEs and LREEs is strong. The HFSE elements including Nb, Ta, Zr, and Hf are strongly depleted (Fig. 6). The tectonic setting discrimination data (Fig. 11)

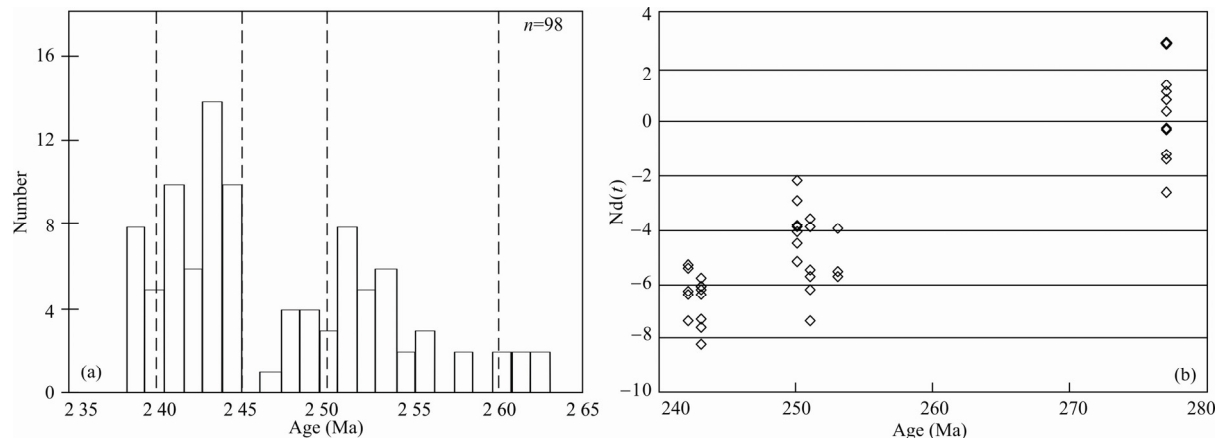


Fig. 12. (a) Age probability diagram for 277–240 Ma magmatite in the EKOB; (b) Distribution diagram for 277–240 Ma intermediate-basic pluton in the EKOB.

Data for 277–240 Ma magmatite are from (Chen Hongwei et al., 2004; Yang Jingsui et al., 2005; Sun Yu et al., 2009; Wang Song et al., 2009; Xiong Fuhao et al., 2011; Li et al., 2012; Xiong et al., 2012, 2013, 2014; Zhang et al., 2012; Chen Guochao, 2014; Huang et al., 2014; Liu et al., 2014; Xia et al., 2014, 2015a, 2015b; Chen et al., 2015; Li et al., 2015; Luo Mingfei et al., 2015). Data for 277–245 Ma intermediate-basic magmatite are from (Chen Hongwei et al., 2005; Xiong et al., 2012, 2013, 2014; Zhang et al., 2012; Ma Changqian et al., 2013; Huang et al., 2014; Liu et al., 2014; Xia et al., 2015b).

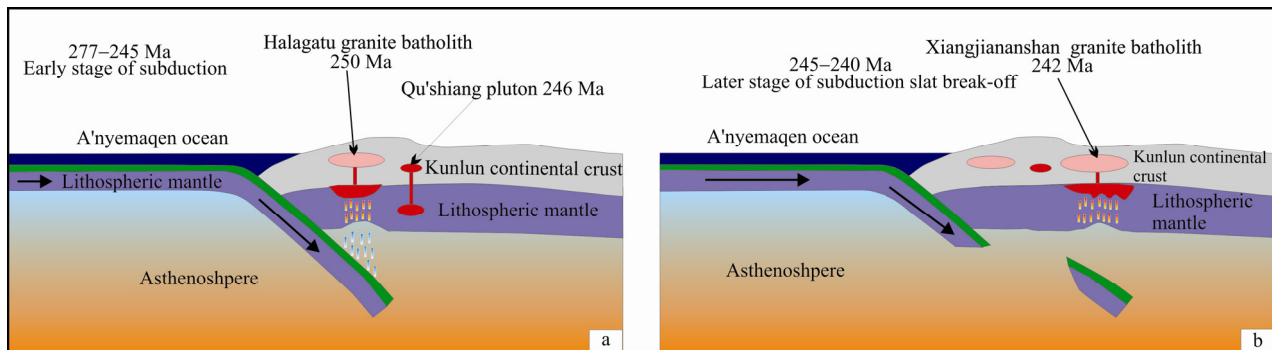


Fig. 13. Schematic diagrams illustrating the tectonic and magmatic evolution of the eastern part of the EKOB during the subduction stage.

obviously suggest island-arc-magma characteristics in the early stage, whereas the late stage is more similar to those formed in an intraplate environment. In the Th/Yb–Nb/Yb diagram (Fig. 8a), there is higher enrichment in the late magma than in the early magma. These results demonstrate that mantle metasomatism from subduction fluids was weaker during the early stage of subduction. However, the mantle metasomatism from later subduction fluids increased with continuous subduction. The Middle Permian–Early Triassic mafic magma isotopes in the EKOB have similar geochemical trends. The  $\epsilon\text{Nd}(t)$  is relatively higher in the early-stage magma and the average value is  $-2.73$  and  $-6.3$  in the late-stage magma (Fig. 12b). These values suggest that the mantle metasomatism from subduction fluids increased.

The data suggest that the geodynamics of Middle Permian–Early Triassic magmatism in the EKOB can be divided into two stages.

(1) Early-stage subduction caused the early magmatism and upward fluid intrusions that induced mantle melting. The product, such as mafic magma and fluids underplated the crust and formed arc magmatic rocks in 277 Ma–245 Ma (Fig. 13a).

(2) In the late stage, magmatism continued for a short time, but it was more extensive. Obvious magmatic mixing is linearly distributed in an east–west direction. Such strong magmatic activity over a short period of time can reasonably be explained by slab break-off during late subduction (Fig. 13b). In 245 Ma–240 Ma, the continuous subduction of oceanic crust increased the density of eclogite-facies rocks and caused the oceanic crust to break off and sink. This led to rapid mantle upwelling to reduce the pressure and formed the mafic magma. Simultaneously, a large amount of felsic magmas formed owing to underplating. The formation age of the QSG is 246 Ma, which is the critical evolution period of the EKOB in Late Paleozoic–Early Mesozoic and the transitional stage from early subduction to late slab break-off.

## 7 Conclusions

Zircon U–Pb dating yields  $246.61 \pm 0.62$  Ma for the crystallization age of granodiorite and  $245.45 \pm 0.9$  Ma of the MME. The porphyritic diorite represents partial melts of lithospheric mantle that were modified by subduction metasomatic fluids. The granodiorite was formed by the fractional crystallization of intermediate–basic magma that evolved to porphyritic diorite. The middle Early Triassic is a critical period during the Late Paleozoic–Early Mesozoic tectonic evolution of the EKOB and the transitional stage from early subduction to late slab break-off.

## Acknowledgements

This study was jointly supported by the National Science Foundation of China (Grant No., 41472191, 41502191, 41172186, 40972136), the Special Fund for Basic Scientific Research of Central Colleges, Chang'an University (Grant Nos. 310827161002, 310827161006), the Commonweal Geological Survey, the Aluminum Corporation of China and the Land-Resources Department of Qinghai Province (Grant No., 200801). We appreciate anonymous reviewers for their thorough and constructive comments which greatly improved the quality of the manuscript. Gao Jingmin, Wu Shukuan, Wei Fanghui, Yang Jie, Li Xiaobing and Wei Bo are thanked for their help during the field work.

Manuscript received July 20, 2016

accepted Sept. 20, 2016

edited by Fei Hongcai

## Reference

- Aldanmaz, E., and Pearce, J.A., Thirlwall, M.F., and Mitchell, J.G., 2000. Petrogenetic evolution of late Cenozoic, post-collision volcanism in western Anatolia, Turkey. *Journal of Volcanology and Geothermal Research*, 102: 67–95.
- Anderson, T., 2002. Correction of common Pb in U–Pb analyses that do not report  $^{204}\text{Pb}$ . *Chemical Geology*, 192(1–2): 59–79.

- Boynton, W.V., 1984. *Geochemistry of the rare earth elements: meteorite studies*. In: Henderson P ed. *Rare earth element geochemistry*. Amsterdam Elservier, 63–114.
- Castillo, P.R., 2008. Origin of the adakite high-Nb basalt association and its implications for postsubduction magmatism in Baja California, Mexico. *Geological Society of America Bulletin*, 120: 451–462.
- Chen Guochao, Pei Xianzhi, Li Ruibao, Li Zuochen, Pei Lei, Liu Zhanqing, Chen Youxin, Liu Chengjun, Gao Jingming and Wei Fanghui, 2013a. Zircon U-Pb Geochronology Geochemical Characteristics and Geological Significance of Cocco A'Long Quartz Diorites Body from the Hongshuichuan Area in East Kunlun. *Acta Geologica Sinica*, 87(2): 178–196 (in Chinese with English abstract).
- Chen Guochao, Pei Xianzhi, Li Ruibao, Li Zuochen, Pei Lei, Liu Zhanqing, Chen Youxin, Liu Chengjun, Gao Jingming and Wei Fanghui, 2013b. Late Triassic magma mixing in the East Kunlun Orogenic Belt: A case study of Helegang Xilikete granodiorites. *Geology in China*, 40(4): 1044–1064 (in Chinese with English abstract).
- Chen Guochao, Pei Xianzhi, Li Ruibao, Li Zuochen, Pei Lei, Liu Zhanqing, Chen Youxin, Liu Chengjun, Gao Jingming and Wei Fanghui, 2013c. Geochronology and genesis of Helegang Xilikete plutons from south margin of eastern part in East Kunlun Orogenic Belt and their geological significance. *Acta Geologica Sinica*, 87(10): 1524–1541 (in Chinese with English abstract).
- Chen Guochao, 2014. *Petrology, Genesis and Geological Significance of Late Palaeozoic-Early Mesozoic Granites in East Kunlun Orogen*. Xi'an: University of Chang'an (Ph. D thesis): 1–221 (in Chinese).
- Chen Guochao, Pei Xianzhi, Li Ruibao, Li Zuochen, Liu Chengjun, Chen Youxin, Xu Tong and Zhang Yongming, 2016. Genesis of magma mixing and mingling of Xiangjiananshan granite batholith in the eastern section fo East Kunlun Orogen. *Earth Science Frontiers*, 23(4): 226–240 (in Chinese with English abstract).
- Chen Hongwei, Luo Zhaohua, Mo Xuanxue, Liu Chengdong and Ke Shan, 2005. Underplating mechanism of Triassic granite of magma mixing origin in the East Kunlun Orogenic Belt. *Geology in China*, 32(3): 386–395 (in Chinese with English abstract).
- Chen Nengsong, Sun Ming, Wang Qingyan, Zhao Guochun, Chen Qiang and Shu Guiming, 2007. EMP chemical ages of monazites from Ccentral Zone of the eastern Kunlun orogen: Records of multi-tectonometamorphic events. *Chinese Science Bulletin*, 52(11): 1297–1306 (in Chinese).
- Chen, X.H., Gehrels, G., Yin, A., Zhou, Q., and Huang, P.H., 2015. Geochemical and Nd-Sr-Pb-O isotopic constrains on Permo-Triassic magmatism in eastern Qaidam Basin, Qinghai-Tibetan plateau: Implications for the evolution of the Paleo-Tethys. *Jouran of Asina Earth Sciences*, 114: 674–692.
- Condie, K.C., Frey, B.A., and Kerrich, R., 2002. The 1.75Ga Iron King Volcanics in westcentral Arizona: a remnant of an accreted oceanic plateau derived from a mantle plume with a deep depleted component. *Lithos*, 64: 49–62.
- Dai, J.G., Wang, C.S., Hourigan, J., and Santosh, M., 2013. Multi-stage tectono-magmatic events of the East Kunlun Range, northern Tibet: Insights from U-Pb geochronology and (U-Th)/He thermochronolgy. *Tectonophysics*, 599: 97–106.
- Defant, M.J., and Drummond, M.S., 1990. Derivation of some modern magmas by melting of young subducted lithosphere. *Nature*, 347: 662–665.
- Dahlquist, J.A., 2002. Mafic microgranular enclaves: early segregatin from metaluminous magma (Sierra de Chepes). Pampean Ranges, NW Argentina. *Journal of South America Earth Science*, 15: 643–655.
- Ding, Q.F., Jiang, S.Y., and Sun, F.Y., 2014. Zircon U-Pb geochronology, geochemical and Sr-Nd-Hf isotopic compositions of the Triassic granite and diorite dikes form the Wulonggou mining area in the East Kunlun Orogen, NW China: Petrogenesis and tectonic implications. *Lithos*, 205: 266–283.
- Donaire, T., Pascual, E., Pin, C and Duthou, J.L., 2005. Microgranular enclaves as evidence of rapid cooling in granitoid rocks: the case of the Los Pedroches granodiorite, Iberian Massif, Spain. *Contributions to Mineralogy and Petrology*, 149(3): 247–265.
- Feng Chengyou, Wang Song, Li Guochen, Ma Shengchao and Li Dongsheng, 2012. Middle to Late Triassic granitoids in the Qimantang area, Qinghai Province, China: Chronology, geochemistry and metallogenetic significances. *Acta Petrologica Sinica*, 28(2): 665–678 (in Chinese with English abstract).
- Hart, S.R., and Zindler, A., 1986. In search of a bulk-Earth composition. *Chemical Geology*, 57(3): 247–267.
- Huang, H., Niu, Y.L., Nowell, G., Zhao, Z.D., Yu, X.H., Zhu, D.C., Mo, X.X., and Ding, S., 2014. Geochemical constraints on the petrogenesis of granitoids in the East Kunlun Orogenic Belt, northern Tibetan Plateau: Implications for continental crust growth through syn-collisional felsic magmatism. *Chemical Gelog*, 370: 1–18.
- Jian Ping, Chen Yuqi and Liu Dunyi, 2001. Petrographical study of Metamorphic Zircon: Basic roles in interpretation of U-Pb age of high grade Metamorphic rocks. *Earth Science Frontiers*, 8(3): 183–191 (in Chinese with English abstract).
- Johnson, K.T.M., 1994. Experimental cpx/and garnet/melt partitioning of REE and other trace elements at high pressure, petrogenetic implication. *Mineralogy Magazine*, 58: 454–455.
- Kinzel, R.J., 1997. Melting of mantle peridotite at pressures approaching the spinel to garnet transition: application to midocean ridge basalt petrogenesis. *Journal of Geophysical Research*, 102: 853–874.
- Langmuir, C.H., Vocke, R.D., Hanson, G.N., and Hart, S.R., 1978. A general mixing equation with applications to Icelandic basalts. *Earth and Planetary Science Letters*, 37: 380–392.
- Li Bile, Sun Fengyue, Yu Xiaofei, Qian Ye, Wang Guan and Yang Yankun, 2012. U-Pb dating and geochemistry of diorite in the eastern section from eastern Kunlun middle uplifted basement and granitic belt. *Acta Petrologica Sinica*, 28(4): 1163–1172 (in Chinese with English abstract).
- Li Huakun, Zhu Shixing, Xaing Zhengqun, Su Wenbo, Lu Songnian, Zhou Hongying, Gen Jijianzhen, Li Sheng and Yang Fengjie, 2010. Zircon U-Pb dating on tuff bed from Gaoyuzhuang Formation in Yanqing, Beijing: Further constraints on the new subdivision of the Mesoproterozoic stratigraphy in the northern North China Craton. *Acta Petrologica Sinica*, 26(7): 2131–2140 (in Chinese with English abstract).
- Li Ruibao, Pei Xianzhi, Li Zuochen, Liu Zhanqing, Chen Guochao, Chen Youxin, Wei Fanghui, Gao Jingming, Liu Chengjun and Pei Lei, 2012. Geological characteristics of Late Palaeozoic-Mesozoic unconformities and their response to some significant tectonic events in eastern part of Eastern Kunlun. *Earth Science Frontiers*, 19(5): 244–254 (in Chinese with English abstract).
- Li, X.H., Li, Z.X., Li, W.X., Liu, Y., Yuan, C., Wei, G.J., and Qi,

- C.S., 2007. U-Pb zircon, geochemical and Sr-Nd-Hf isotopic constraints on age Guangdong, SE China: A major igneous event in response to foundering of a subducted flat-slab? *Lithos*, 96: 186–204.
- Li, X.W., Huang, X.F., Luo, M.F., Dong, G.C., and Mo, X.X., 2015. Petrogenesis and geodynamic implications of the Mid-Triassic lavas from East Kunlun, northern Tibetan Plateau. *Journal of Asian Earth Sciences*, 105: 32–47.
- Li Zuochen, Pei Xianzhi, Liu Zhanqing, Li Ruibao, Pei Lei, Chen Guochao, Liu Chengjun, Chen Youxin, Gao Jingming, Wei Fanghui, Wu Shukuan, Wang Yinchuan and Yang Jie, 2013. Geochronology and Geochemistry of the Gerizhuotuo Diorites from the Buqingshan Tectonic Mélange Belt in the Southern Margin of East Kunlun and Their Geologic Implications. *Acta Geologica Sinica*, 87(8): 1090–1103 (in Chinese with English abstract).
- Liu, B., Ma, C.Q., Zhang, J.Y., Xiong, F.H., Huang, J., and Jiang, H.A., 2014.  $^{40}\text{Ar}$ - $^{39}\text{Ar}$  age and geochemistry of subduction-related mafic dikes in northern Tibet, China: petrogenesis and tectonic implications. *International Geology Review*, 56: 57–73.
- Liu Chengdong, Mo Xuanxue, Luo Zhaohua, Yu Xuehui, Chen Hongwei, Li Shuwei and Zhao Xin, 2004. Crust-mantle magma mixing in East Kunlun: Evidence from zircon SHRIMP chronology. *Chinese Science Bulletin*, 47(6): 596–602 (in Chinese).
- Lu Lu, Hu Daogong, Zhang Yongqing, Wu Zhenhan, 2010. Zircon U-Pb age from syntectonic granitic porphyry in the Middle Kunlun fault belt and its Tectonic significance. *Journal of Geomechanics*, 16(1): 36–43 (in Chinese with English abstract).
- Ludwig, K.R., 2003. Isoplot/Ex, Version 2.49: A Geochronological Tool kit for Microsoft Excel. Berkeley: Berkeley Geochronology Center Special Publication, No 1a: 1–56.
- Luhr, J.F., and Haldar, D., 2006. Barren Island Volcano (NE Indian Ocean): Island-arc high-alumina basalts produced by troctolite contamination. *Journal of Volcanology and Geothermal Research*, 149(3–4): 177–212.
- Luo Mingfei, Mo Xuanxue, Yu Xuehui, Li Xiaowei, Huang Xiongfei and Yu Junchuan, 2014. Zircon LA-ICP-MS U-Pb age dating, petrogenesis and tectonic implications of the Late Triassic granites from the Xiangride area, East Kunlun. *Acta Petrologica Sinica*, 30(11): 3229–3241 (in Chinese with English abstract).
- Luo Mingfei, Mo Xuanxue, Yu Xuehui, Li Xiaowei and Huang Xiongfei, 2015. Zircon U-Pb geochronology, petrogenesis and implication of the Later Permian granodiorite from the Wulonggou Area in East Kunlun, Qinhai Province. *Earth Science Frontiers*, 22(5): 182–195 (in Chinese with English abstract).
- Maniar, P.D., and Piccoli, P.M., 1989. Tectonic discrimination in granitoids. *Geological Society of America Bulletin*, 01: 635–643.
- Ma Changqian, Xiong Fuqiao, Zhang Jinyang, Liu Bin, Huang Jian and Jiang Hongan, 2013. The Effects of Subduction Plate of Magmatism in the Stage of Plate Subduction to Post-Tectonic: Evidence of Mafic Dike of Early Permian–Late Triassic East Kunlun. *Acta Geologica Sinica*, 87(Z1): 79–81 (in Chinese with English abstract).
- Martin, H., 1999. Adakitic magmas: modern analogues of Archaean granitoids. *Lithos*, 46: 411–429.
- McCulloch, M.T., and Gamble, J.A., 1991. Geochemical and geodynamical constraints on subduction zone magmatism. *Earth and Planetary Science Letters*, 102(3–4): 358–374.
- McKenzie, D., and O'Nions, R.K., 1991. Partial melt distribution from inversion of rare earth element concentrations. *Journal of Petrology*, 32: 1021–1091.
- Meng, F.C., Zhang, J.X., and Cui, M.H., 2013. Discovery of Early Paleozoic eclogite from the East Kunlun, Western China and its tectonic significance. *Gondwana Research*, 23: 825–836.
- Mo Xuanxue, Luo Zhaohua, Deng Jinfu, Yu Xuehui, Liu Chengdong, Chen Hongwei, Yuan Wanming and Liu Yunhua, 2007. Granitoids and Crustal Growth in the East-Kunlun Orogenic Belt. *Geological Journal of China Universities*, 13 (3): 403–414 (in Chinese with English abstract).
- Moyen, J.F., 2009. High Sr/Y and La/Yb ratios: the meaning of the “adakitic signature”. *Lithos*, 112: 556–574.
- Mullen, E.D., 1983. MnO/TiO<sub>2</sub>/P<sub>2</sub>O<sub>5</sub>: A minor element discriminant for basaltic rocks of oceanic environments and its implications for petrogenesis. *Earth and Planetary Science Letters*, 62(1): 53–62.
- Pearce, J.A., 1982. Trace element characteristics of lavas from destructive plate boundaries. In: Thorpe, R.S. (ed.), *Orogenic andesites and related rocks*. Chichester, John Wiley and Sons: 528–548.
- Pearce, J.A., 2008. Geochemical fingerprinting of oceanic basalts with applications to ophiolites classification and the search for Archean oceanic crust. *Lithos*, 100, 14–48.
- Pei Xianzhi, Hu Nan, Liu Chengjun, Li Ruibao, Li Zuochen, Chen Youxin, Pei Lei, Liu Zhanqing, Chen Guochao and Yang Jie, 2015. Detrital Composition, Geochemical Characteristics and Provenance Analysis for the Maerzheng Formation Sandstone in Gerizhuotuo Area, Southern Margin of East Kunlun Region. *Geological Review*, 61(2): 307–323 (in Chinese with English abstract).
- Rapp, R., and Watson, E.B., 1995. Dehydration melting of metabastal at 8–32 kbar: implications for continental growth and crust-mantle recycling. *Journal of Petrology*, 36: 891–931.
- Ren, H.D., Wang, T., Zhang, L., Wang, X.X., Huang, H., Feng, C.Y., Teschner, C., and Song, P., 2016. Age, Sources and Tectonic Setting of the Triassic Igneous Rocks in the Easternmost Segment of the East Kunlun Orogen, Central China. *Acta Geologica Sinica* (English Edition), 90(2): 641–668.
- Rollinson, H.R., 1993. *Using geochemical data: evaluation, presentation, interpretation*. New York: Longman Group UK Ltd, 1–352.
- Sun, S.S., and McDonough, W.F., 1989. Chemical and isotopic systematics of oceanic basalts: Implications for mantle composition and processes. In: Sunders A.D., and Norry, M.J. (eds.), *Magmatism in the Ocean Basins*. London: Geological Society of London, 313–345.
- Sun Yu, Pei Xianzhi, Ding Sanping, Li Ruibao, Feng Jianyun, Zhang Yafeng, Li Zuochen, Chen Youxin, Zhang Xiaofei and Chen Guochao, 2009. Halagatu Magma Mixing Granite in the East Kunlun Mountains—Evidence from Zircon U-Pb Dating. *Acta Geologica Sinica*, 83(7): 1000–1010 (in Chinese with English abstract).
- Wang Guocan, Zhang Tianping, Liang Bin, Chen Nengsong, Zhu Yunhai and Bai Yongshan, 1999. Composite ophiolitic melange zone in central part of Eastern section of Eastern Kunlun orogeny and Geological significance of “Fault belt in central part of Eastern section of Eastern Kunlun orogeny”. *Earth Science—Journal of China University of Geosciences*, 24(2): 129–133 (in Chinese with English abstract).

- Wang Song, Feng Chenyong, Li Shijin, Jiang Junhua, Li Dongsheng and Su Shengshun, 2009. Zircon SHRIMP U-Pb dating of granodiorite in the Kaerqueka polymetallic ore deposit, Qimantage Mountain, Qinghai Province, and its geological implications. *Geology in China*, 36(1): 74–84 (in Chinese with English abstract).
- Walter, M.J., 1998. Melting of garnet peridotite and origin of komatiite and depleted lithosphere. *Journal of Petrology*, 39: 29–60.
- Wedepohl, K.H., 1995. The composition of the continental crust. *Geochimica et Cosmochimica Acta*, 59(7): 1217–1232.
- Weyer, S., Muenker, C., and Mezger, K., 2003. Nb/Ta, Zr/Hf and REE in the depleted mantle: Implications for the differentiation history of the crust-mantle system. *Earth and Planetary Science Letters*, 205(3): 309–324.
- Wilson, M., 1989. *Igneous Petrogenesis*. London: Unwin Hyman Press. 295–323.
- Wu Fuyuan, Li Xianhua, Yang Jinhui and Zhen Yongfei, 2007. Discussions on the petrogenesis of granites. *Acta Petrologica Sinica*, 23(6): 1217–1238 (in Chinese with English abstract).
- Wu Zhenhan, Ye Peisheng, Zhao Wenjin, Patrick J. Barosh and Hu Daogong, 2007. Late Cenozoic overthrust system in the southern East Kunlun Mountains, China. *Geological Bulletin of China*, 26(4): 448–456 (in Chinese with English abstract).
- Xia Rui, Qing Min, Wang Changming and Li Wenliang, 2014. The Genesis of the Ore-Bearing Porphyry of the Tuoketuo Porphyry Cu Au(Mo) Deposit in the East Kunlun, Qinghai Province: Constraints from Zircon U Pb Geochronological and Geochemistry. *Journal of Jilin University (Earth Science Edition)*, 44(5): 1502–1524 (in Chinese with English abstract).
- Xia, R., Wang, C.S., Deng, J., Carranza, E.J.M., Li, W.L., and Qing, M., 2014. Crustal thickening prior to 220Ma in the East Kunlun Orogenic Belt: Insights form the Late Triassic granitoids in the Xiao-Nuomuhong pluton. *Jouranl of Asian Earth Sciences*, 93: 193–210.
- Xia, R., Wang, C., Qing, M., Deng, J., Carranza, E.J.M., Li, W.L., Guo, X.D., Ge, L.S., and Yu, W.Q., 2015a. Molybdenite Re-Os, zircon U-Pb dating and Hf isotopic analysis of the Shuangqing Fe-Pb-Zn-Cu skarn deposit, East Kunlun Mountains, Qinghai Province, China. *Ore Geology Reviews*, 66: 114–131.
- Xia, R., Wang, C.S., Qing, M., Li, W.L., Carranza, E.J.M., Guo, X.D., Ge, L.S., and Zeng, G.Z., 2015b. Zircon U-Pb dating, geochemistry and Sr-Nd-Pb-Hf-O isotopes for the Nan' getan granodiorites and mafic microgranular enclaves in the East Kunlun Orogen: Record of closure of the Paleo-Tethys. *Lithos*, 234–235: 47–60.
- Xiong Fuqiao, Ma Changqian, Zhang Jinyang and Liu Bin, 2011. LA-ICP-MS zircon U-Pb dating, elements and Sr-Nd-Hf isotope geochemistry of the Early Mesozoic mafic dyke swarms in East Kunlun Orogenic Belt. *Acta Petrologica Sinica*, 27(11): 3350–3364 (in Chinese with English abstract).
- Xiong, F.H., Ma, C.Q., Zhang, J.Y., and Liu, B., 2012. The origin of mafic microgranular enclaves and their host granodiorites from East Kunlun, Northern Qinghai-Tibet Plateau: implications for magma mixing during subduction of Paleo-Tethyan lithosphere. *Mineralogy and Petrology*, 104: 211–224.
- Xiong, F.H., Ma, C.Q., Jiang, H.A., Liu, B., Zhang, J.Y., and Zhou, Q., 2013. Petrogenetic and tectonic significance of Permian calc-alkaline lamprophyres, East Kunlun orogenic belt, Northern Qinghai-Tibet Plateau. *International Geology Review*, 55(14): 1817–1834.
- Xiong, F.H., Ma, C.Q., Zhang, J.Y., Liu, B., and Jiang, H.A., 2014. Reworking of old continental lithosphere: an important crustal evolution mechanism in orogenic belts, as evidenced by Triassic I-type granitoids in the East Kunlun orogen, Northern Tibetan Plateau. *Journal of the Geological Society*, 171: 847–863.
- Xu Zhiqin, Li Haibing and Yang Jingsui, 2006. An orogenic plateau—the orogenic collage and orogenic types of the Qinghai-Tibet plateau. *Earth Science Frontiers*, 13(4): 1–17 (in Chinese with English abstract).
- Xu Zhiqin, Yang Jingsui, Li Wenchang, Li Huaqi, Cai Zhihui, Yan Zhen and Ma Changqian, 2013. Paleo-Tethys system and accretionary orogen in the Tibet Plateau. *Acta Petrologica Sinica*, 29(6): 1847–1860 (in Chinese with English abstract).
- Yang Jingsui, Xu Zhiqin, Li Haibing and Shi Rendeng, 2005. The paleo-Tethyan volcanism and plate tectonic regime in the Anyemaqen region of East Kunlun, Northern Tibet Plateau. *Acta Petrologica Et Mineralogica*, 24(5): 36–380 (in Chinese with English abstract).
- Yin Hongfu and Zhang Kexin, 1997. Characteristics of the Eastern Kunlun Orogenic belt. *Earth Science—Journal of China University of Geosciences*, 22(4): 339–342 (in Chinese with English abstract).
- Yin Hongfu, Zhang Kexin and Chen Nengsong, 2003. *The People's Republic of China Regional Geologica Report: Donggi Congag Hu Map(I47C001002)*, Scale: 1:25000. Wuhan: China University of Geosciences Press, 1–457 (in Chinese).
- Yuan Wanming, Mo Xuanxue, Yu Xuehui and Luo Zhaohua, 2000. The Record of Indosian Tectonic Setting form the Granotoid of Eastern Kunlun Mountains. *Geological Reviews*, 46(2): 203–211 (in Chinese with English abstract).
- Zhang, H., Ma, C.Q., Xiong, F.H., Jiang, H.A., Liu, B., and Guo P., 2016. Two Contrasting Ophiolites in One Suture Zone: a Case Study form East Kunlun Orogenic Belt, North Tibetan Plateau. *Acta Geologica Sinica (English Edition)*, 89(suppl.2): 111–112.
- Zhang, J.Y., Ma, C.Q., Xiong, F.H., and Liu, B., 2012. Petrogenesis and tectonic significance of the Late Permian-Middle Triassic calc-alkaline granites in the Balong region, East Kunlun Orogen, China. *Geological Magazine*, 149(5): 892–608.
- Zhang Zicheng, Zhang Xujiao, Gao Wangli, Hu Daogong, Lu Lu, 2010. Evidence of Zircon U-Pb ages for the formation time of the East Kunlun left-lateral ductile shear belt. *Journal of Geomechanics*, 16(1): 51–58 (in Chinese with English abstract).
- Zhao, J.H., and Zhou, M.F., 2007. Geochemistry of Neoproterozoic mafic intrusions in the Panzhihua district (Sichuan Province, SW China): implications for subductionrelated metasomatism in the upper mantle. *Precambrian Research*, 152: 27–47.

### About the first author

CHEN Guochao Male, born in 1979 in Nanyang City, Henan Province; received his Ph.D's degree in structural geology from Chang'an University in 2014. Now he is working at the Nanyang Institute of Technology and Chang'an University Geological Resources and Geological Engineering post doctoral research station, and focus on the granitoid and structural geology. Email: chaoschen@126.com.